2 HXN: NANOPROBE BEAMLINE

2.1 Executive Summary

The proposed beamline design follows many of the ideas presented in the December 2006 NSLS-II CDR with additional operation modes. Determining an optics plan for this beamline is complicated by the fact that the required final optics for achieving 1nm focal spots do not yet exist. The uncertainty associated with the optics requires that the beamline be designed with sufficient flexibility to provide the necessary contingency to accommodate an eventual optics solution. The challenge is to provide this flexibly without paying an excessive cost premium or the need to rebuild/replace components—allowing on-budget and on-time completion of the beamline. The design detailed here incorporates this flexibly and controls risk by utilizing well-understood front end and FOE optics components to deliver the x-ray beams generally required for illuminating any successful nano-focusing optics.

The plan is based on two focal points: one at 41 m and the other at 76 m, both supplied by a common set of upstream optics that are located in the front end and FOE. At each of these two locations a hutch will house the necessary end station equipment to support the scientific goals of the beamline. The exact location of these hutches will be determined by a number of factors, such as the characteristics of the final nano-focusing optics and details involving conventional facilities (floor space, roof line, egress, utilities, etc.). One way to look at this proposed layout is to consider the 41 m hutch a 1x location and the 76 m hutch a 2x location with regard to beam demagnification. Operationally, the focused x-ray beam can be used in only one hutch at a time. A beam stop located at the back wall of the upstream 1x hutch would allow access to the downstream 2x hutch while beam is present in the 1x hutch. Access to the 2x experimental location during x-ray operation of the 1x location will allow off line work to be performed using the end station equipment. Given the sophistication and complexity of a nano probe end station, this will provide valuable access time for instrumentation development and testing, as well as experiment setup.

The 1x/2x hutch arrangement will play a key role during the early operation phase of the project, when the main activity will be optics testing and commissioning. During this initial phase and well before the 2x hutch (and transport to it) is completed, the 1x location will serve as an early test location where various optics approaches can be evaluated and refined for eventual use in the push to 1 nm in the 2x hutch. There also exists the possibly of achieving a 1nm focal spot at the 1x location if modes such as a waveguide-coupled aperture prove feasible. The two locations can also be instrumented with complimentary end station equipment such as a full-field imaging system in the 1x location providing flexibly and agility in meeting the demands of the user science program.

The optics report section describes five optics modes: two for the 76 m 2x location, and three for the 41 m 1x location. The proposed support optics will be used to configure these five modes and are general enough to provide additional operation modes if necessary. They are also well understood today regarding both performance and cost.

Particular attention should also be given to address vibration issues with the building experimental and outbuilding floor and the principle optical items—namely, the Monochromator and Mirror systems and other key diagnostic and sample hardware. Similarly, the scanning table supports will have to be state-of-he art vibration isolated systems. Novel solutions should also be sort for BPM systems these need to be nanometer accuracy and supported upon thermally stable and vibration-free supports.

2.2 Scientific Objective

This beamline will allow the study of nanomaterials, which play important roles today in many diverse scientific fields, opening up a wide range of scientific problems ranging from studying the structure and function of catalytic nanoparticles, to the mapping of strain in buried grain boundaries, to determining the structure of single molecule devices.

This hard x-ray nanoprobe beamline will be designed and optimized to enable the production and use of a beam of hard x–ray photons with a nm beam size. As such, it will be a world-leading instrument, enabling spatially resolved versions of many powerful structural and spectroscopic x-ray techniques with unprecedented resolution. In particular, it will allow the study of nanomaterials which today play important roles in many diverse scientific fields. This beamline will take maximum advantage of the low emittance beam provided by the NSLS-II lattice.

The primary experimental techniques for this beamline will likely be scanning nanobeam techniques, but it will also have a limited full-field capability. The limited full-field capability will assist in rapidly locating areas of interest, and would thus allow more efficient use of beam time. For the scanning probe techniques, there are a variety of contrast mechanisms that allow one to extract useful information from the real-space mapping of a sample. For example, one can spatially resolve the density, elemental composition, crystallographic phase, strain, texture, chemical state, local atomic environment, and magnetization. It will operate in a number of modes, each of which will place different requirements on the detectors.

In the first mode, a fluorescence detector can be used with the sample to reveal the spatial distribution of individual elements. The second mode will use a large-area, low-spatial resolution high-sensitivity detector, such as a CCD, to obtain a spatial map of selected Fourier components of a crystallographic phase, and also a spatial map of the local strain. Third, by scanning the incident photon energy, it will be possible to access a number of spectroscopic quantities, such as the local environment from EXAFS and the local chemical state from XANES. Finally, from the back-scattered Compton scattering, one can measure the electron density. This will be especially useful for light elements such as carbon.

2.3 Insertion Device

For the nanoprobe, the over-riding design guidance is to improve the chances of attaining a 1 nm spot size. In order to do this, it is clear that the low-beta insertion section with the small source size is the right choice.

2.3.1 Undulator Power

Power density calculations have been performed for an undulator using equations presented by Kim.[1] Table 2.1 details the source, undulator, and beam parameters. Note that these calculations were prepared for a U19 cryogenically cooled permanent magnet device. We currently anticipate that the standard device for NSLS-II baseline hard x-ray undulators will be a room-temperature U20 In proceeding further with the design for this beamline, this choice should be further re-optimized and these calculations performed again.

Table 2.1. Source, Undulator, and Beam Parameters.

Source parameters	Source energy, E_s	3 GeV
	Source current, I	500 mA
Undulator parameters	Period length, λ_u	19 mm
	Number of periods	158
	Deflection parameter, K	2.03
Beam parameters	Horizontal electron size, σ_x	38.5 μm
	Horizontal electron divergence, σ'_x	14.2 μrad
	Vertical electron size, σ_y	3.05 μm
	Vertical electron divergence, σ'_y	3.22 μrad

Normalization factor, G(K). The normalizing factor is defined as:

$$G(K) = K \cdot \frac{(K^6 + 24/7 \cdot K^4 + 4 \cdot K^2 + 16/7)}{(1 + K^2)^{7/2}} \tag{2-1}$$

Substitute known values and calculate the normalization factor.

$$G(K) = (2.03) \cdot \frac{((2.03)^6 + 24/7 \cdot (2.03)^4 + 4 \cdot (2.03)^2 + 16/7)}{(1 + (2.03)^2)^{7/2}} = 0.982 \tag{2-2}$$

Magnetic field strength, B_0. The magnetic field strength of the undulator is defined as:

$$B_0 = \frac{K}{0.934 \cdot \lambda_u}. \tag{2-3}$$

Substitute known values and calculate magnetic field strength.

$$B_0 = \frac{2.03}{0.934 \cdot (19 * mm)} = 1.144 Tesla \tag{2-4}$$

Gamma of synchrotron, γ. The gamma parameter is defined as:

$$\gamma = \frac{E_s}{m_e \cdot c^2} \tag{2-5}$$

where E_s=source energy, m_e=mass of the electron (9.1095 x 10^{-28}grams) and c=speed of light (2.99792458 x 10^{10}cm/sec). Substitute known values and calculate the gamma parameter.

$$\gamma = \frac{3GeV}{(9.1095 * 10^{-28} grams) \cdot (2.99792458 * 10^{10} cm/\sec)^2} = 5871 \tag{2-6}$$

Power density distribution, $P_u(\theta, \psi)$. Power density in the forward direction is given by:

$$P_u(\theta,\psi) = 10.84 \cdot B_0 \cdot {E_s}^4 \cdot I \cdot N \cdot G(K) \cdot f_K(\theta,\psi) \quad (2\text{-}7)$$

where I = source current and N = number of periods. Based on the source, undulator, and beam parameters (Table 2.1) and the detailed functions, Figure 2.1 plots the incident vertical and horizontal heat flux distributions.

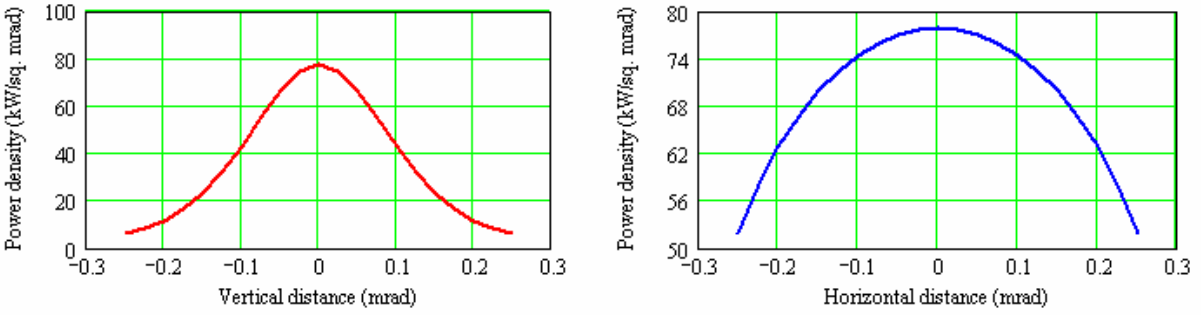

Figure 2.1. Heat flux distributions for the U20 undulator.

2.4 Sector Layout

2.4.1 Front-End Layout

In this section, the components in the front end (upstream of the ratchet wall) are discussed.

2.4.1.1 Front End Differential Pump Mask (FEDPM)

This power limiting mask will allow approximately 90% of the undulator harmonic (at 1 Å) to pass, reduces the total power to a level that is more manageable by the downstream components and protects against mis-steering of the electron beam. It will be located behind the shield wall as close to the undulator as possible with the next component (Front End Defining Aperture Mask, FEDAM) directly downstream. The vertical and horizontal location of this critical component will be defined through survey with additional motorized horizontal positioning over a restricted range to aide the initial alignment of the orbit (its front end location will make it difficult to access manual adjustors). Due to its location and size, this component is ideal for acting as the vacuum conduction-limiting aperture for a differential pump, freeing up space in the optics enclosure.

- distance from source = 14 m
- positioning = Y manual, X motorized (±0.5 mm)
- number of motors = 1

2.4.1.2 Front End Defining Aperture Mask (FEDAM)

To provide some thermal control of the central beam, motorized translation of the FEDPM and the FEDAM will be included to allow the horizontal beam size to be restricted to match the effective vertical coherent source size during nano-focusing.

- distance from source = 15 m
- aperture size = 0.3 mm (vertical) and 1.1 mm (horizontal)
- positioning = Y manual, X motorized (±0.5 mm)
- number of motors = 1
- percent harmonic (at 1 Å) = 90%
- power transmitted = 130.6W – aperture size = 0.3 mm (vertical) and 1.1 mm (horizontal)
- power transmitted = 35.7W – aperture size = 0.3 mm (vertical) and 0.3 mm (horizontal)

2.3.4.2 Beamline Layout

Figures 2.2, 2.3, and 2.4 outline the proposed beamline layout.

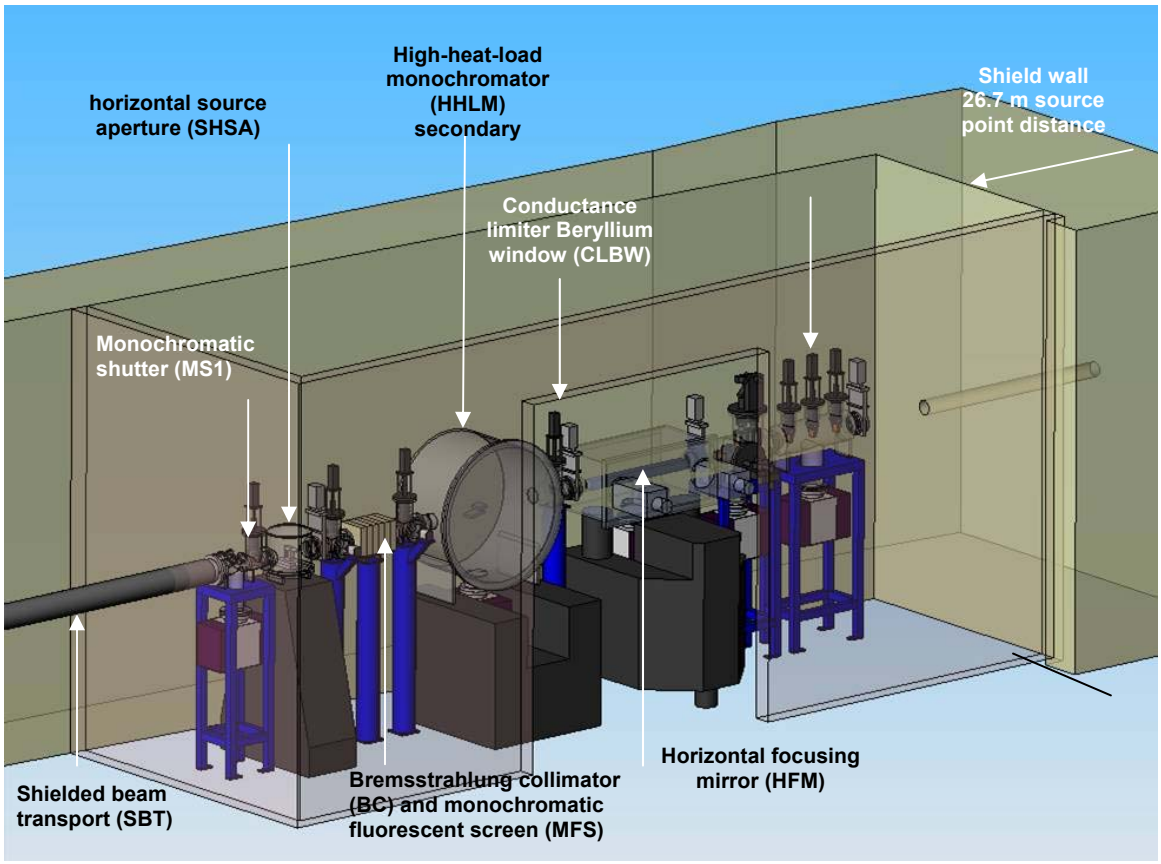

Figure 2.2. Nanoprobe beamline First Optics Enclosure (FOE).

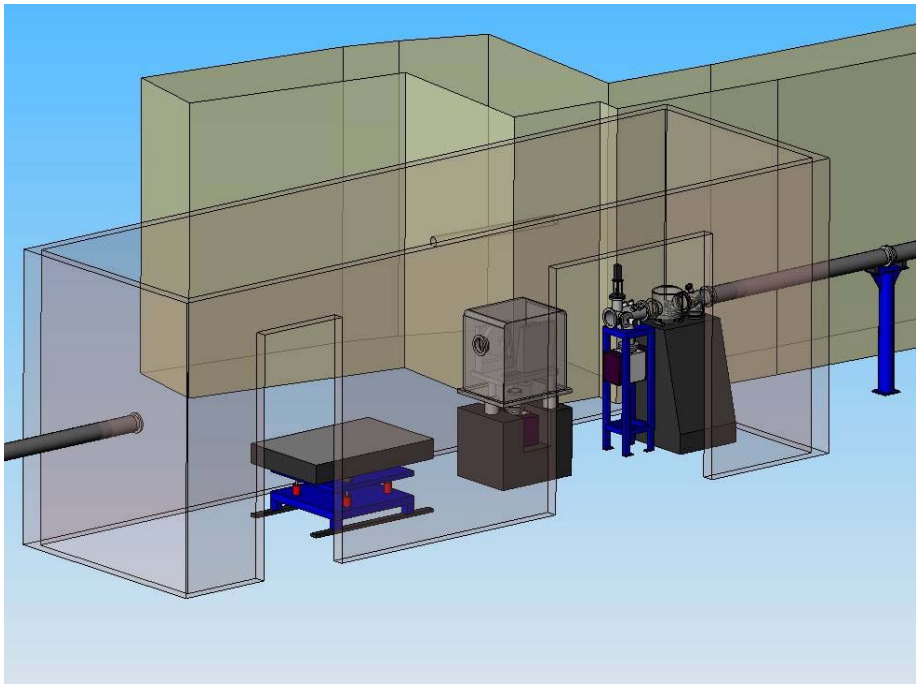

Figure 2.3. Nanoprobe beamline Station A. This station is the “x1” station and is within the experimental hall (see text).

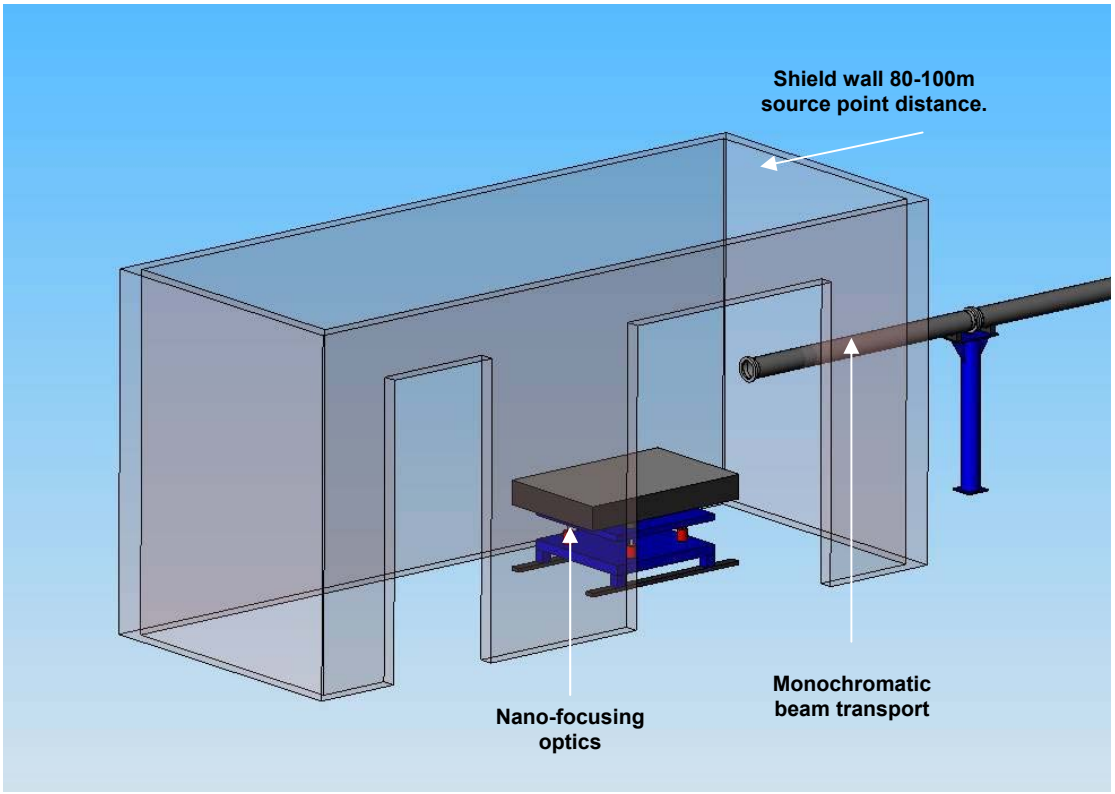

Figure 2.4. Nanoprobe beamline Station B.

2.4.2.1 Survey and Alignment

The NSLS-II nanoprobe sector should commission ~40 survey monuments on the sector, consisting of robust brass monuments countersunk into the floor. In all, there are 20 monuments located on the ID line aligned on the main ID centerline. These monuments, along with additional vertical wall marks and egress aisle locations, constitute the principal fiducial reference points for survey and alignment of the beamlines.

In addition, metallic stick-on targets will be located on the floor offset 1 meter to the main monument lines. These can be used to either establish temporary parallel lines for survey or to act as 90° turn-off points. These monuments should be surveyed relative to the two primary NSLS-II monuments per beamline. After installation, as-built precision coordinate measurements of several of the monuments will be made by the NSLS-II survey and alignment team. The locations of the monuments are shown in the main layout.

Survey and Alignment Guides

Survey monuments. Each FOE and Experiment Station will have brass monuments counter-sunk into the floor, at front and rear, plus approximately every three or four m, for each beamline.

The monuments used in NSLS-II will be compatible with the target mount for a laser tracker. The maximum error is typically ±0.3 mm. An adapter cap will fit over the monument for fitting of a 1.5-inch diameter laser retro-reflector.

Beamline centerline. A 0mrad beamline centerline will be placed in every enclosure, described with dedicated scribed brass monuments.

Beamline equipment. Each piece of beamline equipment will have mounts for laser tracker targets—typically three per piece of equipment. These should be offset to enable measurements of x-y-z and pitch, roll, and yaw adjustments.

Beamline height: 1.4 m. Each beamline will have dedicated survey targets in every enclosure. Wall-mounted targets are very useful for independent survey capability of beamline instrumentation using a Leica auto level with an accuracy capability of 10 μm.

Survey target location. Each radiation enclosure will have survey targets positioned at beam height at front and rear, plus every 3 m, for each beamline. The survey targets will be mounted on the hutch wall or concrete wall.

NSLS-II survey monuments. NSLS-II will provide a pattern of survey monument floor reference locations. These will typically be in the egress aisles plus at other key locations.

Cartesian coordinate framework. All major experimental equipment shall be kinematically mounted on the experimental floor. This will provide the ability to measure complete Cartesian coordinate reference information for experimental equipment. Provision will be made for survey reference floor markings in experiment stations, plus two target spheres on experimental equipment.

Survey Equipment

Survey equipment that has been ascertained to be available for local alignment and survey is as follows.

Beamline height instrumentation. Auto-Leveler - Nikon (accuracy of the scale division ±0.1 mm). The following upgrade may be implemented to achieve 10μm accuracy:

- NA2 Precision Auto Leveler
- GPM3 Parallel plate 10 mm for NA2
- GST-20 Tripod
- GVO-10 Short Focus lens for NA2 (1.8 m – 0.9 m)

Bragg motion axis. Survey targets are to be provided on all Bragg axes, such the device can be aligned to beam height and perpendicular to the beam centerline patch

2.4.2.2 Utility Layouts

Table 2.2 details the estimated coolant usage for the front end and first optics enclosure.

Table 2.2 Coolant Usage – Front End and FOE.

Module	Component description	Source point distance	Coolant	Required flow
1	Front End Differential Pump Mask (FEDPM)	14 m	H_20	8 L/min
	Front End Defining Aperture Mask (FEDAM)	15 m		
	Shield Wall	26.7 m		
2	White Beam Filters (WBF)	27.3 m	H_20	4 L/min
3	White Beam Slits (WBS)	27.8 m	H_20	4 L/min
4	Horizontal Focusing Mirror (HFM)	28.8 m	H_20	4 L/min
5	Conductance Limiter Beryllium Window (CLBW)	29.6 m	H_20	4 L/min
6	High Heat Load Monochromator (HHLM)	30.4 m	H_20	4 L/min
	White Beam Monitor (WBM)		LN_2	4 L/min
		30.9 m	H_20	4 L/min
			H_20	32 L/min
	TOTAL		LN_2	4 L/min

Table 2.3 details the estimated motor usage for the front end and first optics enclosure.

Table 2.3 Motor List – Front End and FOE.

Module	Component description	Source point	Number of motors	Motor	Amps / phase
1	Front End Differential Pump Mask (FEDPM)	14 m	1	Stepper	1.4
	Front End Defining Aperture Mask (FEDAM)	15 m	1	Stepper	1.4
3	White Beam Slits (WBS)	27.8 m	1 (horizontal position)	Stepper	1.4
			1 (horizontal aperture)	Stepper	1.4
			1 (vertical position)	Stepper	1.4
			1 (vertical aperture)	Stepper	1.4
4	Horizontal Focusing Mirror (HFM)	28.8 m	2 (mirror incidence)	Stepper	3.0
			3 (mirror alignment)	Stepper	2.0
			2 (mirror bending)	Stepper	2.5
6	High Heat Load Monochromator (HHLM)	30.4 m	1 (Bragg axis)	Stepper	2.5
			3 (2^{nd} crystal – roll, pitch and yaw)	Stepper	0.6
			1 (2^{nd} crystal vertical translation)	Stepper	2.5
	White Beam Monitor (WBM)	30.9 m	1	Stepper	1.4
	Secondary Horizontal Source Aperture (SHSA)	32.0 m	1 (horizontal position)	Stepper	1.4
			1 (horizontal aperture)	Stepper	1.4
	TOTAL		21	Stepper	49.8

2.4.2.3 Life Safety Code Compliance

Egress Aisles. Egress aisles are shown on the architectural layout drawing NSL-100-10-0003-A. All aisles are approximately 44 inches (1.12 m) wide.

2.4.2.4 Beamline Vacuum System

Most of the beamline components will be built to ultra high vacuum specifications with, in general, no vacuum-to-coolant joints. The exception to this are the silicon crystal mount monochromators in the ID beamlines, these will use a Cajon Swagelok VCR-type coupling connected to flexible pipes, for easy connection to the coolant supply.

To isolate the beamline vacuum from machine front end, there will be a differential pumped mask together with a Beryllium window conductance-limiter system. The nanoprobe beamline will utilize ion pumps to pump all beamline sections. In addition, gate valve pumping ports will be used to isolate the monochromator sections, to enable fast pumpdown via permanently installed turbo pump sets. Vacuum will be in the 10^{-7} to 10^{-8} Torr range. All mirror tanks will be isolated by gate valves from the rest of the beamline and will be operated in UHV (~10^{-9} Torr).

Beryllium Window Design

The main design points of the assembly are:

- At least two window thicknesses will be installed between the beamline termination window and the front end, to comply with regulations on the protection of machine vacuum. One thickness is the Be window conductance limiter and the second is the end window.
- The window material will be Brush Wellman IF1. The purity of the Be will be preferentially selected to 99.3% Be assay, with the iron and copper content less than 300 ppm, respectively.
- Coherence of the beam is a significant issue for nanoprobe experiments, so the Be windows will be polished.
- For ID beamline termination windows utilizing white beam, to protect against ozone-induced oxidization and corrosion we intend to investigate the possibility of sub-micron coating with aluminium. Alternatively, we will cap the end of the window flange with a Kapton window and flow dry nitrogen into the inter-space between the Kapton and Be to prevent corrosion. Holes burned into the Kapton due to white beam should be small, and a marginal positive pressure of dry nitrogen should suffice to keep air out and ozone production to a minimum.

Main Vacuum Sections (see also Table 2.4)

Vacuum Section 1

- Pneumatic DN200 all-metal valve (at end of the front end) 10″ CF, 8″ tube
- Tube incorporating machine protection measures: pirani gauge, cold cathode gauge, RGA, right-angled all-metal valve, 300 L/s (nom) ion pump fitted to the tube.
- Graphite Filter and Primary Slits Section – 300 L/s (nom) ion pump
- Pneumatic DN100 all-metal valve

Vacuum Section 2

- Horizontal mirror – water-cooled Si mirror
- 500 L/s (nom) ion pump, pirani gauge, cold cathode gauge, right-angled metal valve

- Diagnostics section (fluorescent screen, tungsten wire)
- Pneumatic DN100 all-metal valve

Vacuum Section 3

- Beryllium conductance-limiter window
- Double crystal monochromator – liquid nitrogen cooled
- Fitted with 500 L/s (nom) ion pump, pirani gauge, cold cathode gauge, right-angled metal valve
- Turbo dry and scroll backing pump fitted to DCM chamber
- Diagnostics section: white beam monitor and mono fluorescent screen
- GB collimator
- Pneumatic DN100 all-metal valve

Vacuum Section 4

- Photon shutter, possibly integrated gas bremsstrahlung (GB-shielding), fitted with 300 L/s (nom) ion pump, pirani gauge, cold cathode gauge, right-angled metal valve
- Secondary horizontal aperture
- Pneumatic DN100 all-metal valve

Vacuum Section 5

- White beam transport pipe 4 m long - 100mm OD tube
- Diagnostics section (fluorescent screen)
- Integrated gas bremsstrahlung/photon shutter, fitted with 300 L/s (nom) ion pump, pPirani gauge, cold cathode gauge, right-angled metal valve

Vacuum Section 6

- Quad diode BPM
- Diagnostics section (fluorescent screen, tungsten wire)
- Tube fitted with 300 L/s (nom) ion pump, pirani gauge, cold cathode gauge, right-angled metal valve
- Tertiary horizontal aperture

Vacuum Section 7

- White beam transport pipe 4 m long – 100 mm OD tube
- Diagnostics section (mono beam fluorescent screen)
- Tube fitted with 300 L/s (nom) ion pump, pirani gauge, cold cathode gauge, right-angled metal valve
- Pneumatic DN100 all-metal valve
- High-resolution monochromator
- Be window: mirror polished to less than 0.5 μm rms

Vacuum Section 8

- Nano focusing optics
- Long beam transport 29 m long

- 4*300 L/sec ion pumps, pirani gauge, cold cathode gauge, right-angled metal valve
- Be window: mirror polished to less than 0.5 μm rms; end window: Kapton foil protection
- Nano focusing optics

Table. 2.4 Vacuum Equipment Inventory.

Item	Approx Number	Comments
500 L/s (nom) ion pump	2	All major optics (mirror/DCMs)
300 L/s (nom) ion pump	5+3	Long beam transport
240 L/sec turbo and scroll set	2	Monochromators
Pirani gauges	6	Distributed down beamline 1 per vacuum section
Cold cathode gauges (IMG)	6	Distributed down beamline1 per vacuum section
RGA	1	Mirror location
Pneumatic DN100 all-metal valve	5	Distributed down beamline
All-metal right-angled valve	6	At strategic places down beamline (see flow)
Portable rough pump/leak detector	1	Not costed for, but required – assume vacuum loan pool at NSLS-II

2.4.2.5 Data Acquisition System and Motion Control

There are many combinations of control and drive electronics available for beamlines, but some general form factor decisions will reduce the options. The NSLS-II controls group will standardize on the high level control form factor.. The decision involves the balance between extra hardware and software costs verses the availability of existing controls software support (see Chapter 6, Control Systems).

Once the high-level user interface computer system has been determined, one can move down to the motor control options. Again, the synchrotron controls group will probably have a preference. The two main paths are either a simple control card (OMS) or a sophisticated intelligent controller (DeltaTau or Newport XPS). Most beamline axes are single drives that do not require any special features. However, there are exceptions, such as a diffractometer that performs trajectory scans or a monochromator that requires encoder averaging.

The final control decision is the drive amplifiers. There are a wide range on the market, with a wealth of different current ratings and features. For example, when choosing a stepper amplifier card one must chose a step size, current rating, holding current, and DC rail voltage. The choice may also be influenced by the packing density within a rack unit and the availability of spares.

2.4.3 Beamline Components

2.4.3.1 Module 1: Front End Differential Pump Mask (FEDPM)

Distance to center of undulator	14 m

A differential pump assembly will be introduced as the first component in the optics to isolate the beamline vacuum from that of the storage ring. Differential pump assembly will consist of a series of pumps separated from each other and from the UHV region by a flow-restricting aperture. The first aperture in the beamline will be fixed by the FEDPM and the FEDAM (directly downstream of the differential pump assembly), and sets the maximum acceptance of the beamline. This maximum acceptance has been set to correspond with the vertical and horizontal FWHM (full width half maximum) sizes and divergences of the

source. Based on the beam parameters detailed in Table 2.1, the maximum size of the front end aperture is given by:

$$X_1 = 4 \cdot \Sigma_x + 4 \cdot \Sigma'_x \cdot (14m) \approx 1100\,\mu m \qquad \text{Maximum horizontal opening}$$

$$Y_1 = 4 \cdot \Sigma_y + 4 \cdot \Sigma'_y \cdot (14m) \approx 300\,\mu m \qquad \text{Maximum vertical opening}$$

Using the detailed functions given in Section 2.3, the transmitted vertical and horizontal heat flux distributions are shown in Figure 2.5.

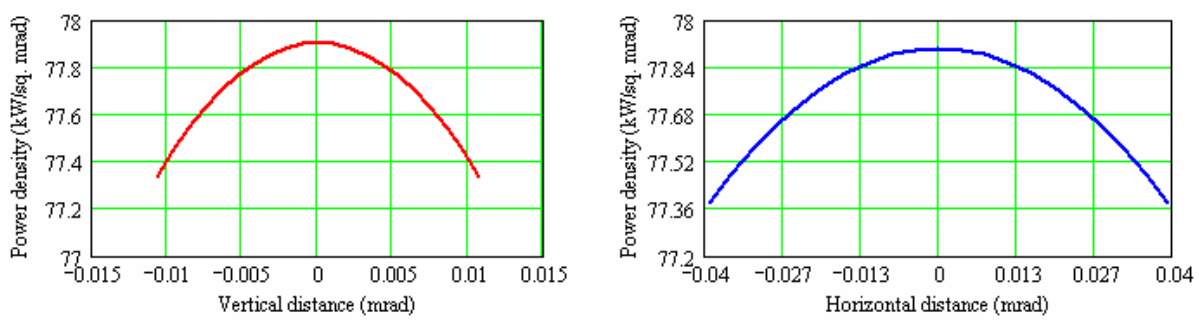

Figure 2.5. Heat flux distributions.

The radiated power for full-field operation is given by:

$$P = \int_{-\left(\frac{0.55mm}{14m}\right)rad}^{\left(\frac{0.55mm}{14m}\right)rad} \left(\int_{-\left(\frac{0.15mm}{14m}\right)rad}^{\left(\frac{0.15mm}{14m}\right)rad} P_u(\theta,\psi)\,d\theta \right) d\psi = 130.6W \ . \qquad (2\text{-}8)$$

This component is a cooled monolithic block of Glidcop AL-15 with a tapered hole terminating in a rectangular aperture with inclined absorber walls to distribute the heat load (Figure 2.6). Before the ingot is machined, it is first explosion-bonded to AISI 304L stainless steel end plates, which are then fixed to short beam tubes and front and rear entrance flanges. Explosion bonding is a bonding method in which the controlled energy of a detonating explosive is used to create a metallurgical bond between two or more similar or dissimilar materials. This joining technique was first utilized at the APS facility to enable high-strength Glidcop AL-15 materials to be used in high-heat-load components for undulator front ends[2]. The explosion bonded ingots are subjected to the standard ultra sonic tests as outlined by APS in LS 237; this is broadly based on the standard ultrasonic procedure ASTM A578, level I.

The total length, flange face to flange face, has been set at 300 mm. The entire assembly is independently mounted on its own scanning platform and can be translated as a unit by ±2 mm horizontal (motorized) and vertically (manual) adjustments to center the mask on the beam.

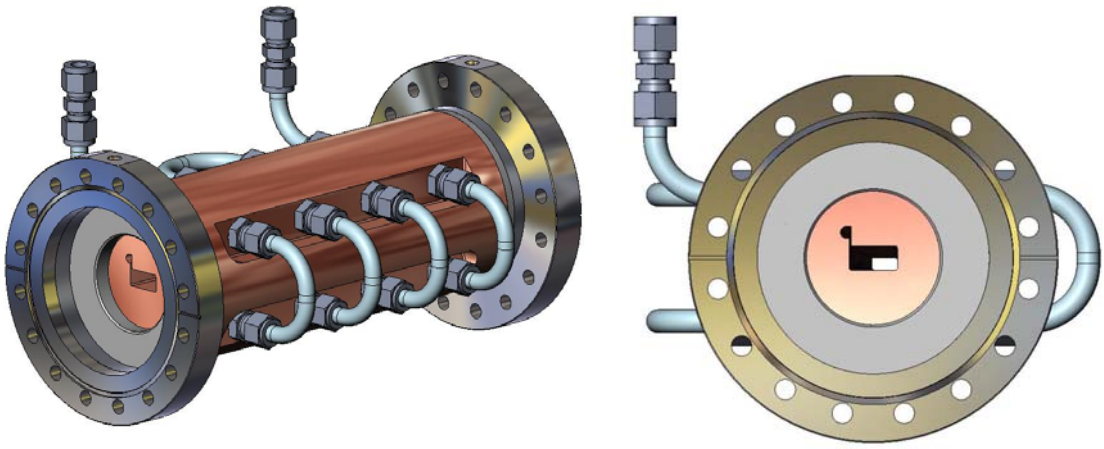

Figure 2.6. Proposed design of the FEDPM.

Motion Specification. Table 2.4 details the required motion specification for the FEDPM assembly.

Table 2.4. Motion Specification for the FEDPM Assembly.

Motion	Range	Resolution	Drive system
Horizontal motorized	±2 mm	<2 μm	Stepper motor driven variable horizontal aperture.
Horizontal manual	±5 mm	0.1 mm	Mask alignment.
Vertical manual	±5 mm	0.1 mm	Mask alignment.
Tilt Φ_X manual	±5°	0.25°	Mask alignment.
Yaw Φ_Y manual	±5°	0.25°	Mask alignment.

2.4.3.2 Module 1: Front End Defining Aperture Mask (FEDAM)

Distance to center of undulator	15 m

To provide some thermal control of the central beam, motorized translation of the FEDPM and the FEDAM will be included to allow the horizontal beam size to be restricted to match the effective vertical coherent source size during nano-focusing. The radiated power for nano-focusing operation is given by:

$$P = \int_{-\left(\frac{0.15mm}{14m}\right)rad}^{\left(\frac{0.15mm}{14m}\right)rad} \left(\int_{-\left(\frac{0.15mm}{14m}\right)rad}^{\left(\frac{0.15mm}{14m}\right)rad} P_u(\theta,\psi)d\theta \right) d\psi = 35.7W \, . \tag{2-8}$$

The proposed design for the FEDAM (Figure 2.7) is identical to that of the FEDPM, with the tapered aperture rotated through 180° along the beam centerline. By moving each aperture section independently in the horizontal direction, a variable-sized rectangular aperture can be created. The entire assembly is independently mounted on its own scanning platform and can be translated as a unit by ±2 mm horizontal (motorized) and vertical (manual) adjustments to center the mask on the beam.

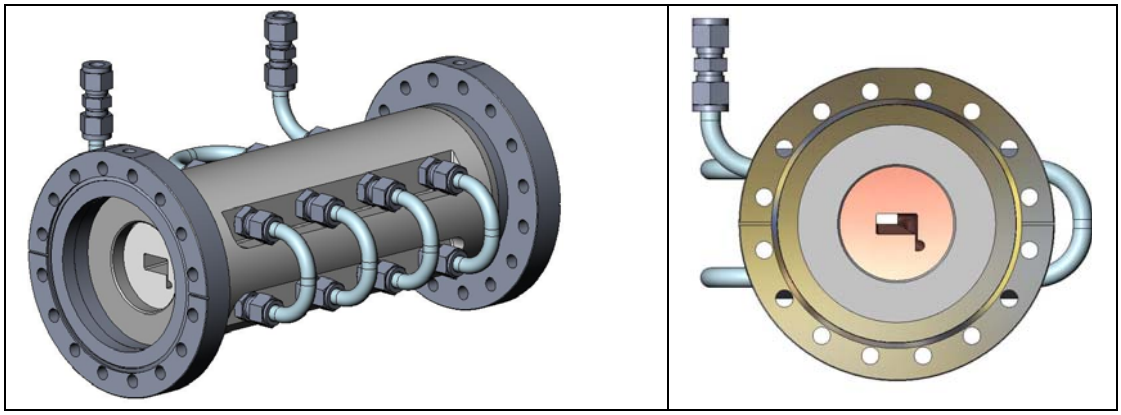

Figure 2.7. Proposed design of the FEDAM.

Motion Specification. Table 2.5 details the required motion specification for the FEDAM assembly.

Table 2.5. Motion Specification for the FEDAM Assembly.

Motion	Range	Resolution	Drive system
Horizontal motorized	±2 mm	<2 µm	Stepper motor driven variable horizontal aperture.
Horizontal manual	±5 mm	0.1 mm	Mask alignment.
Vertical manual	±5 mm	0.1 mm	Mask alignment.
Tilt Φ_X manual	±5°	0.25°	Mask alignment.
Yaw Φ_Y manual	±5°	0.25°	Mask alignment.

2.4.3.3. Shield Wall (SW)

Distance to center of undulator	26.7 m

2.4.3.4 Module 2 - White Beam Filters (WBF)

Distance to center of undulator	27.3 m

The functionality of the filter is to provide variable power absorption upstream of critical beamline components. The design incorporates three water-cooled diamond filters of different thicknesses, each mounted on independent pneumatic actuators with the facility for position translation of the filter in the beam. Diamond filter material is preferred, but there exists uncertainty regarding the degree to which this filter will preserve the source brilliance. There are a number of different types of diamond available, with the best choice for persevering coherence requiring further study. This uncertainty and the need for research and development translate into budget uncertainty. For the purpose of these specifications, commercially available CVD diamond pricing is used.

Based on the source, undulator, and beam parameters, the source spectral power distribution is shown in Figure 2.8. The transmitted spectral power distribution from a 30µm-thick CVD diamond filter is superimposed with the source distribution profile. The transmitted distribution is calculated by multiplying the source spectral distribution with the filter material absorption characteristic. The sum of transmitted

powers at each energy is then divided by the sum of the source power at each energy to give the percentage transmission from the filter. Relative to the source distribution, the power absorption for a 30μm thick CVD diamond filter has been calculated at ~4.1%. Table 2.6 shows foil thickness with calculated absorptions.

Table 2.6. Filter power variation.

Filter thickness (μm)	Transmission (W)	Absorption (W)
30	125.2	5.4
300	107.8	22.8
1000	87.1	43.5

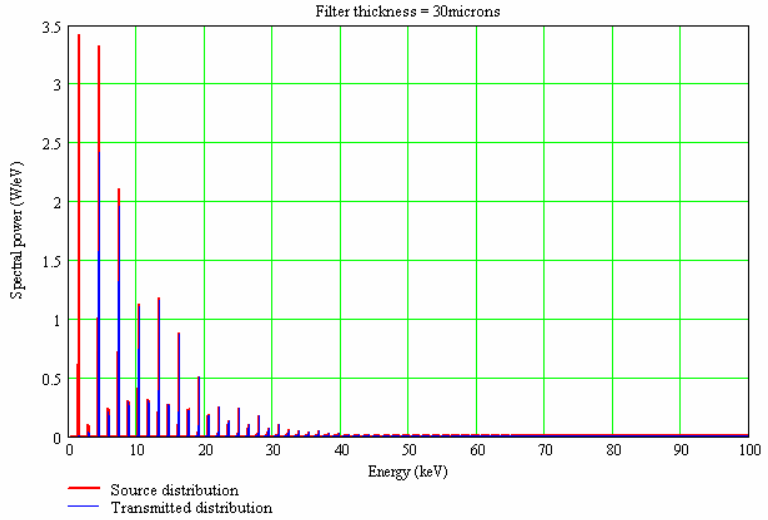

Figure 2.8. Spectral power distributions before and after a diamond filter of 30 microns.

Motion Specification. Table 2.7 details the required motion specification for the WBF assembly.

Table 2.7 Motion Specification for the WBF Assembly.

Motion	Range	Resolution	Drive system
Filter translation	50 mm	<0.5 mm	Pneumatic through vacuum actuator

2.4.3.5 Module 3 - White Beam Slits (WBS)

Distance to center of undulator	27.8 m

The functionality of the primary slits (horizontal and vertical) is to provide an upstream adjustable aperture to regulate the total thermal power exposed to the down stream components. The slits, contained within the same vessel, consist of two actuated jaws positioned serially along the beamline, one mounted horizontally and the other vertically to variably define the beam in the horizontal and vertical direction. Each pair of slits is designed with a single translation drive (up/down for vertical, left/right for horizontal) and with a second drive that adjusts the separation width of the slits (permits precise beam profile measurements with a fixed width slit).

The main design points of the assembly are:

- Each of the slits consists of an inclined block of OFHC copper with a relatively small block of tungsten mounted at the exit end of the slit. Dimensions of slit blade: 80 mm long, 50 mm wide, 30 mm high, and a ~3° incline angle.
- The tungsten edge is precision lapped so that the edge protrudes 0.1 mm above the flat on the OFHC copper incline and defines the beam with a hard edge. The tungsten can be chamfered slightly to further enhance the "hard: defining edge at high energies. The 0.1mm protrusion absorbs very little of the on-axis power density. This "knife-edge" tungsten slit concept has raised no problems in use at sector 13 and 16 at APS.[3, 4]
- The major advantage of this method is that the bulk copper takes the thermal load whilst the tungsten blade provides a hard defining edge for the x-rays.
- The cooling is through copper tubing brazed to the slit blade. No water to vacuum joints.
- The copper blades are mounted in Invar frames for thermal isolation from the support frame and vessel.
- Total length for a pair of actuators (horizontal and vertical) is <50cm.
- The end wall of the chamber can be water cooled to enable any Compton scattering from the slits to be safely absorbed in the chamber walls.
- The drive train has been extensively tested with uni-directional repeatability of 1-2µm and resolution of ~0.5µm. The slits will be equipped with encoders and precision (1micron) limit switches.

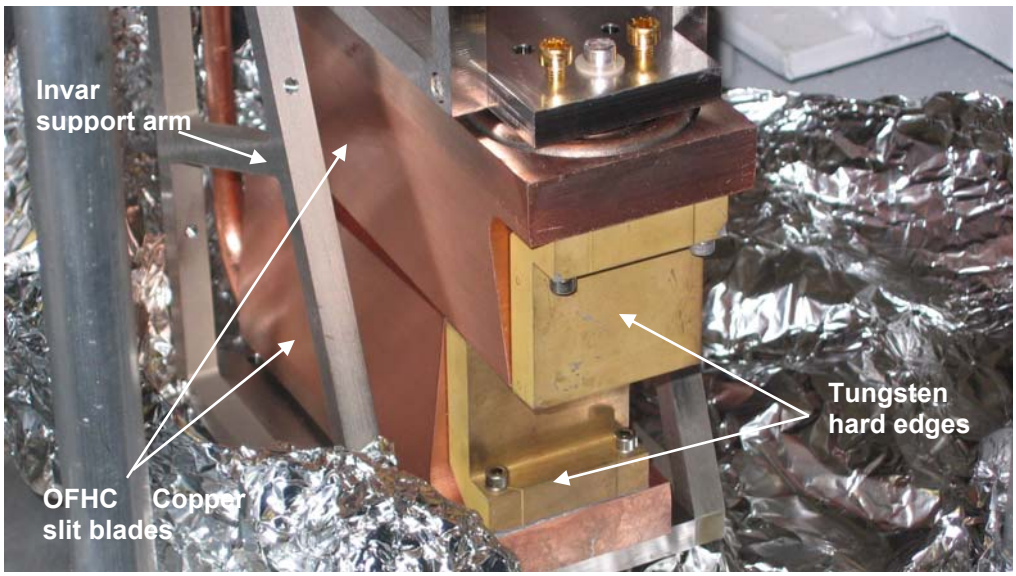

Figure 2.9. High-heat-load slits as used on HXMA ID06 beamline at CLS (designed to operate with >4kW power load).

An FEA model of the slit blade design was run to determine the structural integrity when subjected to the full thermal heat load. To improve the meshing, the FEA model was run with a finer grid than typical, to ensure accurate results. Element sizing can be characterized as fine to very fine, especially around a heat-loaded area and regions considered susceptible to high stress concentrations. The design of the horizontal and vertical slits will be identical; therefore, the incline angle of the slit blades will be fixed by the larger of the horizontal or vertical projected lengths of the beam footprint. The exit aperture of the upstream front end assembly has been set at 1.1 mm (h) by 0.3 mm (v), which at a source point distance of 14 m is equivalent to 78.6 µrad (h) by 21.4 µrad (v). Based on a source point distance of 27.8 m for the white beam slits, the

incident beam is sized at 2.2 mm wide by 0.6 mm high. Therefore, the incline height of the slit blade has been set at 4 mm to allow full acceptance of the beam (including a margin for mis-steer).

When the slit blades are aligned vertically, the incident beam footprint is at a minimum and will therefore produce the highest incident power density. This will be used as the primary design case for the FEA modeling. To apply the thermal load, a small area has been projected onto the optical surface representative of the beam footprint with an applied heat flux 5 W/mm^2 (equivalent to 131 W) to simulate the total thermal load absorbed. Figure 2.10 shows that variation of the horizontal and vertical power densities over the beam footprint are not significant; therefore, using a uniform heat loading for the FEA model is a valid assumption.

Convective cooling has been applied to the feature cut for the brazed coolant pipe. Based on a hydraulic diameter of ~4 mm and a flow rate of 4 L/min, a heat transfer coefficient of 1.8 W/cm^2 K was calculated using the Dittus-Boelter correlation. With the inclusion of thermal contact resistance, the effective heat transfer coefficient on the feature cut has been reduced to 1.5 W/cm^2 K. The results from the thermal models are then loaded into a structural model; with restraints applied to allow free expansion. The results from the FEA model are shown in Figure 2.9.

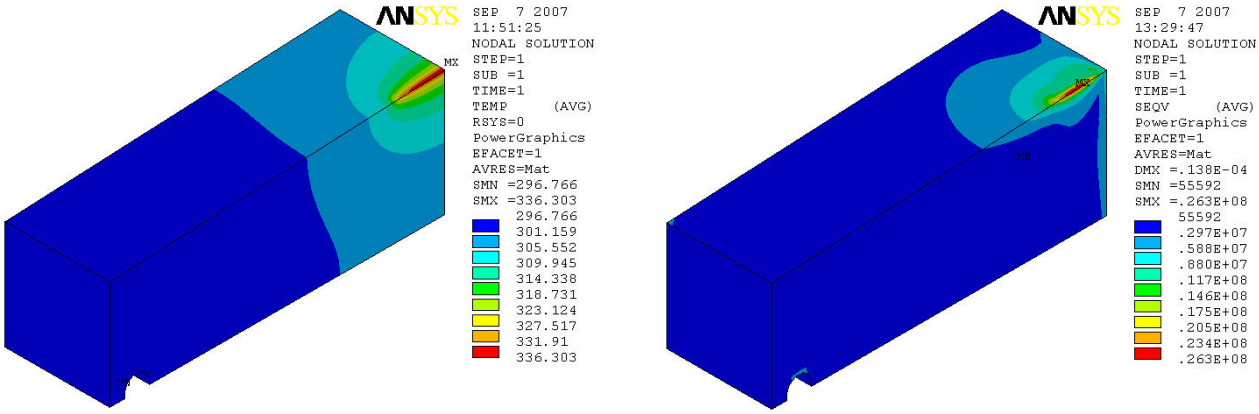

Figure 2.10. Temperature (K) and von Mises stress (Pa) distribution (left and right respectively) of inclined copper block of the white beam slits. The design fatigue stress for OFHC Copper is quoted at 215–254 MPa. The model is therefore not stress critical.

A separate analysis from the main FEA mask model has been undertaken to show the highly localized temperature rise effects on the small at the 0.1mm protrusion of the tungsten jaw into the beam. The 0.1mm element definition required makes the mesh too fine to incorporate into the main mask model. This is a valid model assumption, as the power into the 0.1mm height (by 3.1mm width) is only ~17 W, which makes the local model of the exit aperture almost entirely independent of the main mask model.

- Incident power density = 130.6 W / (2.2 mm x 0.6 mm) = 99 W/mm^2
- Beam footprint area on exit aperture = 0.1 mm x 2. 2 mm = 0.22 mm^2
- Maximum power absorbed into exit aperture = 99 W/mm^2 x 0.22 mm^2 ≈ 22W

To improve the quality of the meshing, the FEA model for the exit aperture was run with a finer grid than is typical, to ensure accurate results. For the thermal model, convective cooling was applied to the contact area between the exit aperture and the slit blade. For reasonable contact pressure exerted by screw fastening (> 4Bar), the effective heat transfer coefficient (representing inverse of thermal resistance) for indium-copper contact[5] is approximately 0.5W/cm^2/K. The bulk temperature for the convective cooling was set to 40°C, this was obtained by probing the contact area from the main FEA model of the slit blade. To apply the thermal load, a small area was projected onto the incident surface and the heat flux (99 W/mm^2) was applied to it. The results from the FEA model are shown in Figures 2.11 and 2.12.

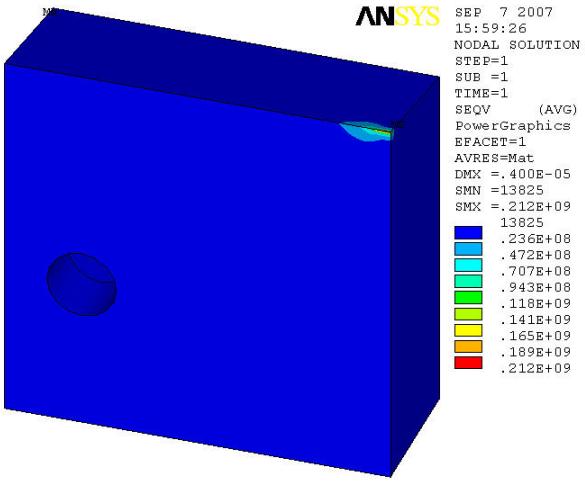

Figure 2.11 Temperature (K) and von Mises stress (Pa) distribution (left and right, respectively) of tungsten jaw of white beam slits. The design fatigue stress for tungsten is quoted at 750 MPa. The model is therefore not stress critical.

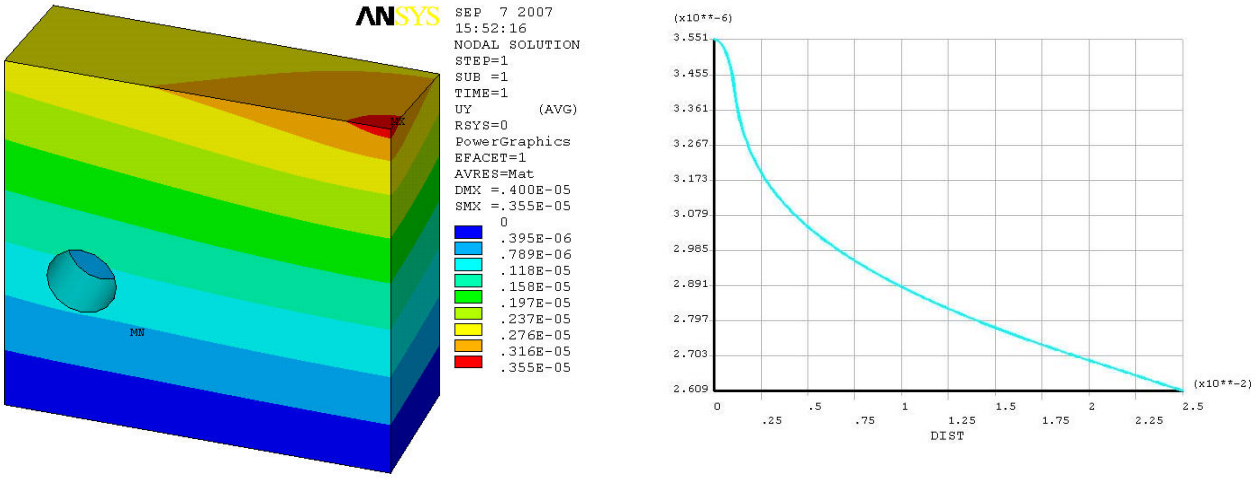

Figure 2.12 Displacement distribution (m) and hard edge displacement profile (m) of tungsten jaw – center at zero (top left and bottom right, respectively). The displacement on the cutting edge is shown to be below 4 microns.

Motion Specification. Table 2.8 details the required motion specification for the WBS assembly.

Table 2.8. Motion Specification for the WBS Assembly.

Motion	Range	Resolution	Drive system
Horizontal and vertical position	±10 mm	<2 µm	Stepper motor driven variable position.
Horizontal and vertical aperture	±5 mm	<0.5 µm	Stepper motor driven variable aperture.

2.4.3.6 Module 4: Horizontal Focusing Mirror (HFM)

Distance to center of undulator	28.8 m

Further power management of the very bright white beam is achieved through a horizontal mirror system. This will be a flat horizontally deflecting mirror used for power management and as a horizontal focusing element in full field mode. To achieve this, two independent moments are applied to either end of the mirror producing a linear moment distribution along the mirror length. The mechanical bender will allow the mirror figure to be corrected for thermal bump when producing unfocused beams as well as allow the horizontal beam to be focused either directly onto the sample or to a secondary horizontal source to be used in a compound focusing mode. In the compound focusing mode nearly the full horizontal source can be made available for full-field imaging.

The principle of the bending mechanism is shown schematically in Figure 2.13. Applying the bending forces to the mirrors through bending holes below the surface allows any distortions resulting from contact strain to dissipate before reaching the optical surface.

The x-ray mirror has two independent functions; suppression of the high energy section of the radiation spectrum and horizontal focusing of the beam. It must be remembered that transmission of photon flux from the source to the sample is the objective of the beamline; therefore reflectivity through the mirror system should be high. The mirror will have an active length of 800 mm, coated with rhodium and bare silicon and operate from 0 – 3 mrad. For low energy reflection (<8 keV), silicon is shown to be an excellent candidate with high reflectivity and harmonic suppression. To maintain mirror reflectivity, a rhodium coating would be used for the operating energies from 8 keV and up.

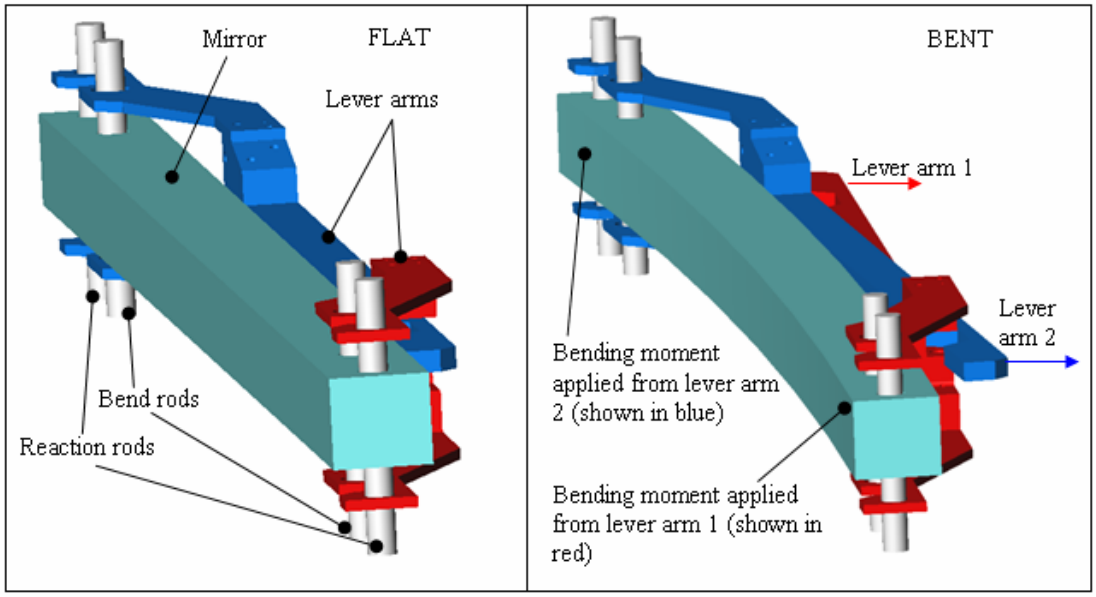

Figure 2.13 Illustrating closed-force bending principle, to be used in horizontal focusing white beam mirror.

Relative to the source distribution (i.e., upstream filters extracted from beam), the mirror power absorption when using each reflective strip is detailed in Table 2.9.

Table 2.9. Mirror Power Absorption, Grazing Angle Set at 3.0 mrad.

Reflective strip	Transmission (W)	Absorption (W)
Silicon	30.9	99.7
Rhodium	80.7	49.9

To determine the mirror displacement due to the thermal heat load, an FEA model of the mirror was run. To improve the quality of the meshing the FEA model for the horizontal mirror has been reduced to half size. Based on the maximum upstream aperture size (differential pump exit aperture), the maximum incident power on the mirror has been calculated at 354 W. To apply the thermal load, a small area has been projected onto the optical surface representative of the beam footprint with an applied heat flux of 213.5 kW/m^2 (equivalent to 130.6 W) to simulate the total thermal load absorbed. Figure 2.6 showed that variation of the horizontal and vertical power densities over the beam footprint are not significant; therefore, using a uniform heat loading for the FEA model is a valid assumption. Convective cooling was applied through the top gallium groove, with an applied heat transfer coefficient of 1 W/cm^2 K. Based on a hydraulic diameter of ~6 mm and a flow rate of 8 L/min, a heat transfer coefficient of 1.5 W/cm^2 K was calculated using the Dittus-Boelter correlation. The heat transfer coefficient value applied inside gallium grooves was lowered to account for the larger wetted area of the grooves relative to the internal area of the coolant pipe. The results from the thermal model are then loaded into a structural model; with restraints applied to allow free expansion. The results from the thermal FEA model are shown in Figure 2.14.

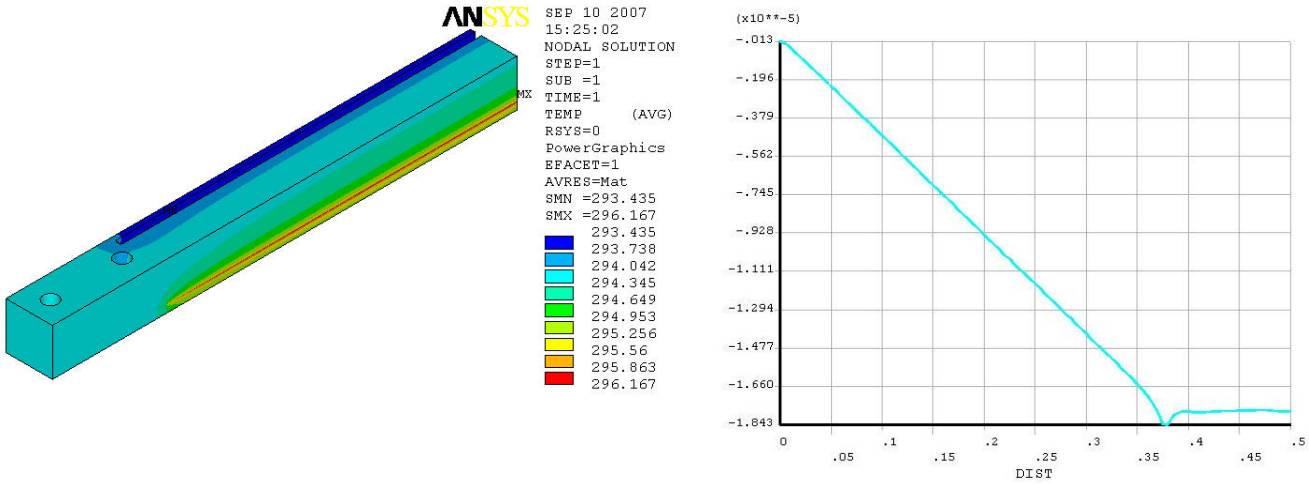

Figure 2.14. Temperature distribution (K) and thermal slope profile (radian) – center at zero (left, top, and right, bottom, respectively).

The ideal mirror bend profile is defined by the focal lengths, the incidence angle, and the optical length of the mirror. To induce the bend and achieve the required central deflection, loads are applied at either end of the mirror through the bending mechanism. However, as thermal bend should also be considered, the bending load applied that is actually applied is calculated to give the corrected mirror profile, as shown in Figure 2.15, taking into account the thermal load.

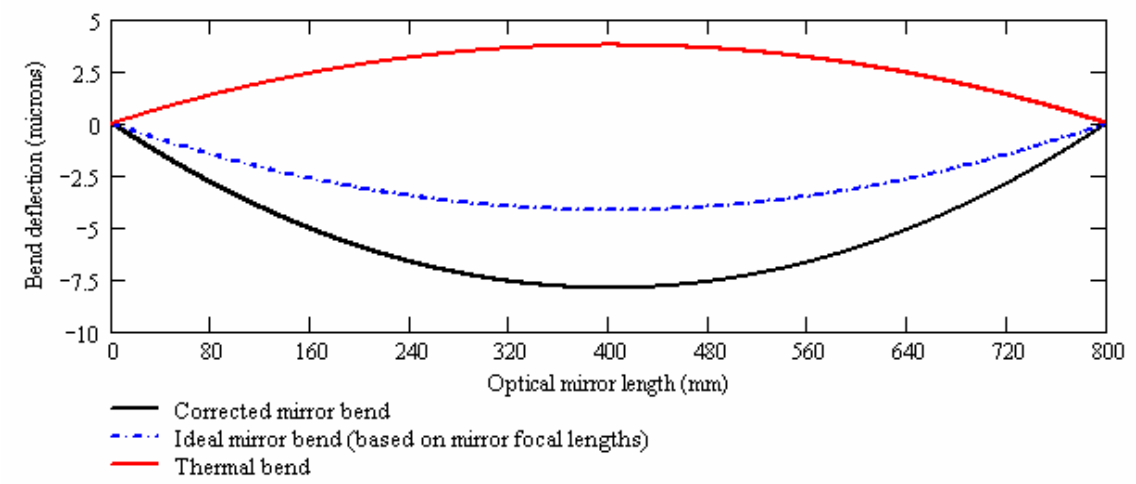

Figure 215. Corrected mirror bend profile, adjusted to include the effects of thermal load.

Since the optical axis normal is perpendicular to the gravity vector (or alternatively expressed, the reflecting optic plane lies parallel to the gravity vector), the requirement for self weight sag appears to be nil. Evidence from previous installations of bent planar mirrors has shown no focus distortion due to possible self weight sag. Based on the corrected mirror bend profile (black line), the deflection at the mid span point along the mirror length was determined. A required bend load of 77 N was then calculated, to give the required deflection at the mid span location. Figure 2.16 superimposes the mirror bend profile (bending loads and thermal bend) with ideal profile based on the mirror's focal length.

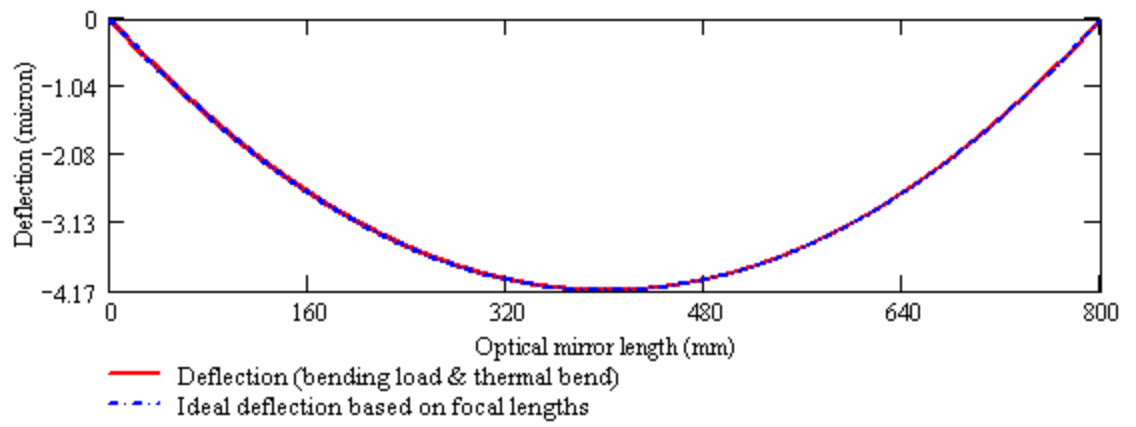

Figure 2.16 Comparison of mirror profiles.

The residual (uncorrectable) slope error is defined as the difference between the mirror slope profile (given by differentiation of its calculated displacement profile) and the slope formed by differentiation of the ideal bend profile (Figure 2.17). The residual slope error of the optically active surface has been corrected to give a root mean squared (RMS) value of 0.32 μrad, calculated over the illuminated length. Note that the optically active area is slightly less than the optical mirror length, due to space taken the bending holes.

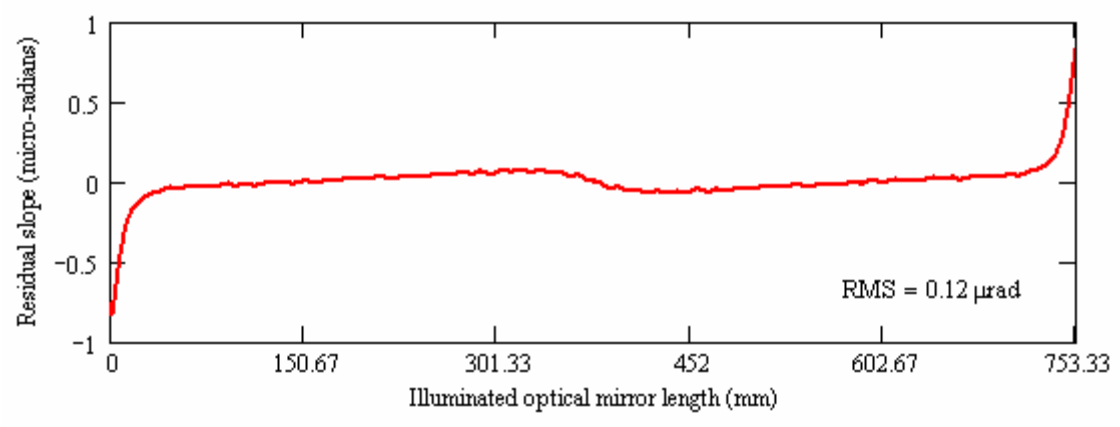

Figure 217 Residual slope error of white beam mirror.

A summary of the key criteria for mirror comparison is given in Table 2.10

Table 2.10 Horizontal Focusing Mirror, Key Criteria.

Description		Focusing mirror, reflecting horizontally
Substrate material		Single crystal silicon
Substrate dimensions		1000 mm long x 50 mm wide x 50 mm deep
Reflective coatings		Rhodium and bare silicon
Focal lengths	F_1	28.8 m
	F_2	∞
Beam acceptance		83 µrad (h) x 56 µrad (v)
Optically active length		754 mm
Incidence angle	θ	3.0 mrad
Radius of curvature	$R = \frac{2}{\left(\frac{\sin(\theta)}{F_1} + \frac{\sin(\theta)}{F_2}\right)}$	19.2 km
Calculated bending load		77 N
Calculated RMS slope error		0.12 µrad
Calculated bending stress	$\sigma = y \cdot \frac{E}{R}$	0.17 MPa

Table 2.11 details the required motion specification for the HFM assembly.

Table 2.11 Motion Specification for the HFM Assembly.

Motion	Range	Resolution	Drive system
Mirror incidence (yaw)	100 mm	<0.05µm	2 stepper motor driven through vacuum actuators.
Motorized fine yaw	±10 µrad	<0.05µrad	Through vacuum piezo driven.
Mirror alignment	±10 mm	<0.2µm	3 stepper motor driven vertical jack systems mounted to base block.
Mirror bending	-10 mm/ +30 mm	<0.2µm	2 stepper motor driven in vacuum actuators.

2.4.3.7 Module 5: Conductance Limiter Beryllium Window (CLBW)

Distance to center of undulator	29.6 m

Located directly upstream of the monochromator, the conductance limiting section is designed to act as a partial vacuum break between the high vacuum (10^{-7} to 10^{-8} Torr) regime in the monochromator and the ultra high vacuum (10^{-9} Torr and better) in the remainder of the beamline. The partial vacuum break is achieved by minimizing molecular flow between regions by providing only very narrow gap between sections, while allowing the beam to pass through (i.e., a vacuum conductance limitation). This is achieved by using an actuated beryllium window such that, when a fixed cooled mask is driven into the beam path, the gap between the frame and the upstream side of the mask is as near zero as possible (~1 mm), limiting the through conductance. There are a number of different designs for mounting the Be foil with the best choice for persevering coherence; these require further study. This uncertainty and the need for research and development translate into budget uncertainty.

Beryllium is a material that is largely transparent to x-rays, and it is therefore well suited to this task, as the beam is affected only in a very small way by passing through. Figure 2.18 shows the mass absorption characteristic for Be, and Figure 2.19 superimposes the transmitted spectral power distribution from the window with the incident distribution profile.

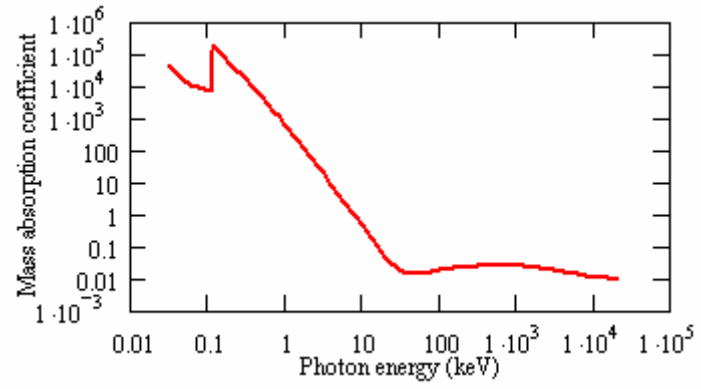

For the 0.003 to 1 KeV energy range, data were taken from:

http://www-cxro.lbl.gov/optical_constants/pert_form.html

For the 1 to 20 MeV energy range, data were taken from:

http://physics.nist.gov/PhysRefData/XrayMassCoef/ElemTab/z04.html

Figure 2.18 Mass absorption characteristic for Be.

The transmitted distribution is calculated by multiplying the incident spectral distribution by the absorption characteristic for beryllium. The sum of transmitted powers at each energy is then divided by the sum of the source power at each energy to give the percentage transmission from the mirror. Relative to the maximum incident heatload (80.7 W – heat load transmitted from the upstream mirror, see Section xx), the power transmission through the window was calculated to be 94.1%.

Motion specification. Table 2.12 details the required motion specification for the Conductance Limiter Beryllium Window assembly.

Table 2.12 Motion Specification for the CLBW Assembly.

Motion	Range	Resolution	Drive system
Filter translation	50 mm	<0.5 mm	Pneumatic through vacuum actuator.

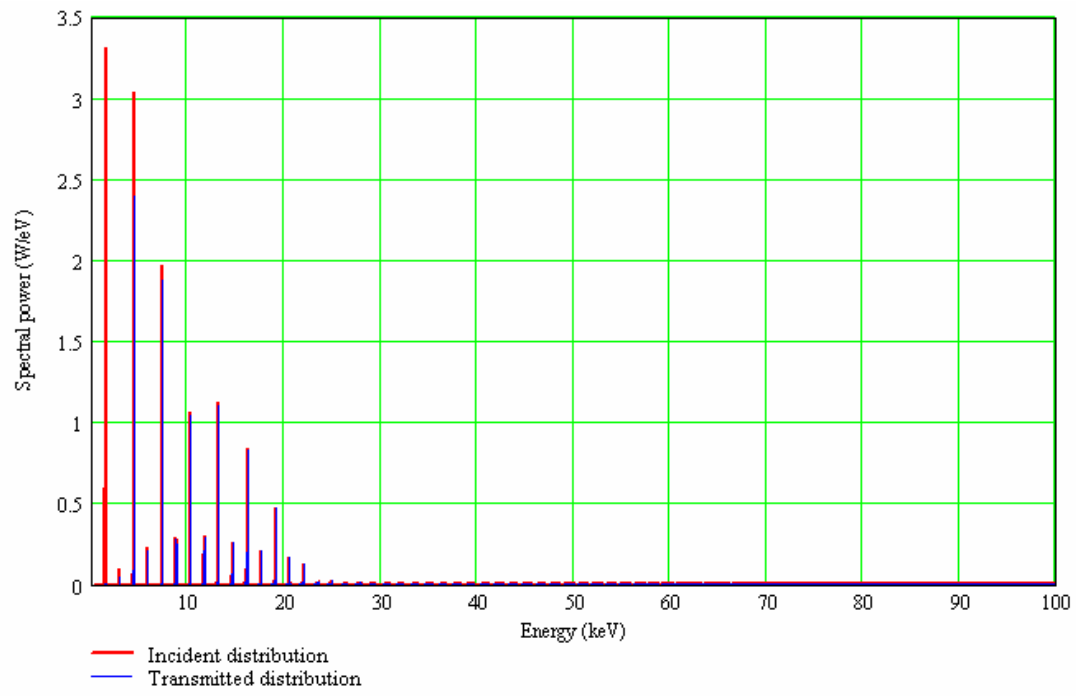

Figure 2.19 Spectral power distributions before and after Be conductance limiter. (Be density = 1850kg/m^3, foil thickness 200 μm).

2.4.3.8 Module 6 - High Heat Load Monochromator (HHLM)

Distance to center of undulator	30.4m

This will be the primary monochromator on the beamline using liquid nitrogen cooled silicon (111) crystals operating with a fixed offset of 20 mm over an energy range of 4 to 24 keV. The energy is changed by rotating the two crystals around a common axis centered on the first crystal surface plane; the output beam height is kept constant by allowing the gap between the faces of the first and second crystal to change (range of motion <1.5 mm) and the beam to "walk" along the surface of a long second crystal. Eliminating the longitudinal translation on the second crystal and replacing it with a long crystal greatly improves ease of tuning energy as well as stability, since the second crystal is more rigidly mounted. Final alignment of the lattice planes of the first and second crystals is achieved with stepper motor-driven actuators for the roll (rotation axis = horizontal axis along the beam), pitch (rotation axis = horizontal axis perpendicular to the

beam) and yaw (rotation axis = vertical axis perpendicular to the beam) adjustment of the second crystal plus a piezoelectric device for the fine pitch and roll adjustment.

Thermal and vibration stability will be of primary importance in this monochromator design. The liquid nitrogen cooling needed to maintain the thermal distortions at acceptable levels has the potential for introducing unacceptable vibration. Managing vibration issues at the level suitable for a nano focus beamline will require research and development effort, including prototypes, and therefore will increase the cost of the final instrument.

The preliminary cooling design for extracting the absorbed heat load is based on the indirect crystal cooling arrangement (similar in principle to that widely used at SPring-8). Since the incident heatload is relatively low, and to improve vibration stability, short lengths of copper braid will be used to connect the liquid nitrogen coolant pipe to the copper blocks. To provide a good thermal contact, indium foil is used between the sides of the silicon crystal and copper blocks. The indium foil has a secondary benefit of absorbing the differential expansion between the copper blocks and silicon crystal and limits the resulting stress and strain transmitted to the silicon at low temperatures. To determine the crystal displacement due to the thermal heat load, an FEA model of the crystal was run. This report shows the FEA results for the silicon crystal only. Element sizing can be characterized as fine to very fine, especially around a heat-loaded area and regions considered susceptible to high-stress concentrations.

To apply the thermal load, a small area has been projected onto the optical surface representative of the beam footprint with an applied heat flux 4.53E+6 W/m^2 (equivalent to 80.7 W – maximum heat load transmitted from upstream mirror, see Section xx) to simulate the total thermal load absorbed. Figure 2.6 showed that variation of the horizontal and vertical power densities over the beam footprint are not significant; therefore, using a uniform heat loading for the FEA model is a valid assumption.

Convective cooling was applied to the cooled contact area between the crystal and the cooled copper heat exchangers. Based the Dittus-Boelter correlation, the heat transfer coefficient through the coolant pipes is given by:

Reynolds number, Re

The Reynolds number is given by:

$$\mathrm{Re} = \rho \cdot \left(\frac{V}{\pi \cdot \left(\frac{D_h}{2} \right)^2} \right) \cdot \left(\frac{D_h}{\mu} \right), \tag{2-9}$$

where

ρ = coolant density (795.52kg/m^3 for liquid nitrogen),

V = volumetric flow rate (4 L/min),

D_h = hydraulic diameter (10 mm), and

μ = dynamic viscosity (0.001465 poise for liquid nitrogen).

Substitute known values and calculate the Reynolds number.

$$\mathrm{Re} = \left(795.52 kg / m^3\right) \cdot \left(\frac{4\, litres/\min}{\pi \cdot \left(\frac{10mm}{2}\right)^2} \right) \cdot \left(\frac{10mm}{0.001465\, poise} \right) = 46092.7 \,. \tag{2-10}$$

Prandtl number, Pr

The Prandtl number is given by:

$$\mathrm{Pr} = \mu \cdot \left(\frac{Cp}{K} \right), \tag{2-11}$$

where Cp = specific heat (2048.2J/kg K for liquid nitrogen) and K = thermal conductivity (0.14086W/m K for liquid nitrogen). Substitute known values and calculate the Prandtl number.

$$\mathrm{Pr} = \left(0.001465\, poise \cdot\right) \left(\frac{2048.2 \frac{J}{kg \cdot K}}{0.14086 \frac{W}{m \cdot K}} \right) = 2.1 \tag{2-12}$$

Nusselt number using the Dittus-Boelter correlation, Nu

For fully developed turbulent flow in smooth tubes, the Nusselt number is defined as:

$$Nu = 0.023 \cdot \mathrm{Re}^{0.8} \cdot \mathrm{Pr}^{0.3} \,. \tag{2-13}$$

Substitute known values and calculate the Prandtl number.

$$Nu = 0.023 \cdot \left(46092.7\right)^{0.8} \cdot \left(2.1\right)^{0.3} = 155.3 \tag{2-14}$$

Heat transfer coefficient through cooling channels, HTC

The heat transfer coefficient is defined as:

$$HTC = \frac{K \cdot Nu}{D_h} \,. \tag{2-15}$$

Substitute known values and calculate heat transfer coefficient.

$$HTC = \frac{\left(0.14086 \frac{W}{m \cdot K}\right) \cdot \left(155.3\right)}{\left(10mm\right)} = 2187.5 \frac{W}{m^2 \cdot K} \,. \tag{2-16}$$

With the inclusion of thermal contact resistance, the effective heat transfer coefficient on the crystal contact surface is given by:

$$HTC = \left[\frac{1}{fa \cdot HTC_0} + \sum R(Cu) + \sum R(In) + Rc \right]^{-1}, \tag{2-17}$$

where

fa = ratio of cooling channel surface area and contact surface area,

HTC_0 = heat transfer coefficient of the coolant in the cooling channels (0.83W/cm^{2}K),

$\sum R(Cu)$ = sum of the thermal conduction resistances in the copper,

$\sum R(In)$ = sum of the thermal conduction resistances in the indium and

Rc = thermal contact resistance at the interface.

As the thermal conductivity of silicon is high at cryogenic temperatures, it is useful to increase the contact surface area by oversizing the crystal height to improve heat transfer (crystal length is limited to prevent interference with the diffracted beam off the second crystal). The ratio of cooling channel surface area and contact surface area is given by:

$$fa = \frac{\text{cooling channel surface area}}{\text{contact surface area}} = \frac{6283.185 mm^2}{7000 mm^2} \approx 0.9 . \tag{2-18}$$

For thicknesses of copper and indium of 3 to 11 mm and 0.5 mm, respectively, the thermal conduction resistance through a single thickness takes the following values:

$$R(Cu) = \begin{pmatrix} 0.75 \\ 2.75 \end{pmatrix} \times 10^{-5} \, m^2 \cdot K \cdot W^{-1} , \tag{2-19}$$

and

$$R(In) = 0.62 \times 10^{-5} \, m^2 \cdot K \cdot W^{-1} . \tag{2-20}$$

Depending on the surface finish, the thermal contact resistance at the interface takes the following values:

$$Rc = \begin{pmatrix} 1 \\ 20 \end{pmatrix} \times 10^{-5} \, m^2 \cdot K \cdot W^{-1} . \tag{2-21}$$

The cooling arrangement includes three copper and two indium interfaces. We substitute known values and calculate heat transfer coefficient at contact surface:

$$HTC = \left[\frac{1}{(0.9) \cdot \left(2187.5 \frac{W}{m^2 \cdot K} \right)} + 3 \times \begin{pmatrix} 0.75 \\ 2.75 \end{pmatrix} \times 10^{-5} \frac{m^2 \cdot K}{W} + 2 \times 0.62 \times 10^{-5} \frac{m^2 \cdot K}{W} + \begin{pmatrix} 1 \\ 20 \end{pmatrix} \times 10^{-5} \frac{m^2 \cdot K}{W} \right]^{-1} \tag{2-22}$$

$$HTC \approx \begin{pmatrix} 1804.4 \\ 1243.5 \end{pmatrix} \frac{W}{m^2 \cdot K}. \tag{2-23}$$

For the FEA model, with the inclusion of thermal contact resistance, the effective heat transfer coefficient on the crystal contact surface has been reduced to 1,200 W/m^2 K. An estimation of the bulk temperature at the contact surface between the crystal and the heat exchanger is given by:

$$T_{crystal\_holder} = \frac{\Delta Q_{Cu}}{K_{Cu}} \cdot \frac{L}{S} \cdot + T_{heat\_exchanger} = \frac{80.7W}{500W/m \cdot K} \cdot \frac{20mm}{300mm^2} + 78K \approx 89K\,, \tag{2-24}$$

where

ΔQ = power dissipated through the copper braids (80.7W),

K_{Cu} = thermal conductivity of copper (500W/m K at cryogenic temperatures),

S = effective section area of braid (300mm^2),

L = braid length (20mm),

$T_{crystal\_holder}$ = temperature at interface between crystal and holder, and

$T_{heat\_exchanger}$ = temperature of liquid nitrogen coolant (78K).

To ensure good thermal contact between the cooled copper block and the silicon crystal, a contact pressure is applied to the side of the copper block, pushing it inward against the silicon crystal. Contact pressure has been set at 350 kPa; this value of contact pressure is based on an approximate relationship of 100 Pa per sq mm of contact area.[6]. This is based on a contact area of 70 mm x 50 mm.

Table 2.13 Summary of Loads Applied to FEA Model.

Case description	E=24 keV	
Thermal model loading	Beam size:	2.26 mm (h) x 0.65 mm (v)
	Heat flux loading:	4.53E+6 W/m^2
	Convection cooling:	HTC = 1200 W/m^2 K
		Bulk temperature = 89 K
Structural model loading	Results from the thermal model are loaded into a structural model, with restraints applied to allow free expansion.	
	Clamping pressure:	350 kPa

Previous thermal analysis of monochromator crystals has shown that the primary design case for selecting the crystal design is generally fixed by the optical performance at the higher energies as a result of the narrower rocking curve widths. The results from the FEA case modeled at 24 keV are shown in Figure 2.20.

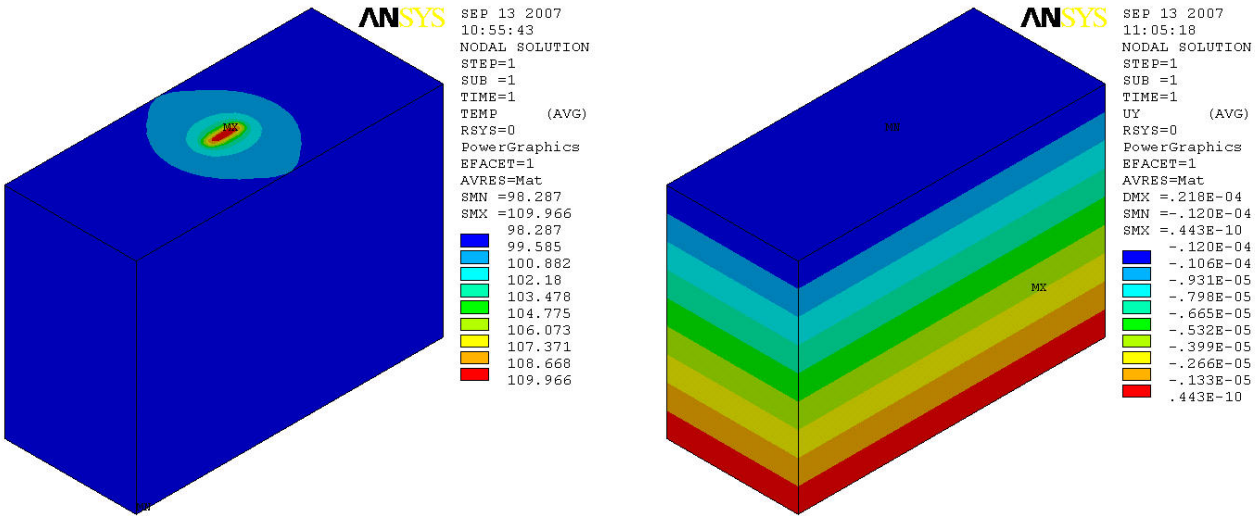

Figure 2.20. Temperature (K) and displacement (m) distribution (left and right, respectively).

To achieve an efficient photon flux transmission at the second monochromator crystal, the slope error on the first crystal should be a fraction of the rocking curve width. Since the rocking curve width is a function of energy, then the slope error for the crystal will also be dependent on the beam's energy. We use this as a basis for a conservative calculation for the first crystal's optical performance. The rocking curve width is the FWHM value for the curve that defines the peak shape on rocking the crystal in the diffracted beam. Assuming a Gaussian curve form, a relative distribution can be determined using the FWHM value. Any slope error on the first crystal surface will result in a shift of this distribution. The quantity of beam reflected is defined by the region shared by the relative distributions, as shown in Figure 2.21. For silicon (111) at 24 keV, the rocking curve width is 11.6 µrad. Based on an integrated reflectivity of 70%, the maximum allowable slope error has been calculated at 3.8 µrad. Approximately 92% of the tangential beam footprint has been shown (Figure.22) to be under the 3.8 µrad slope error limit.

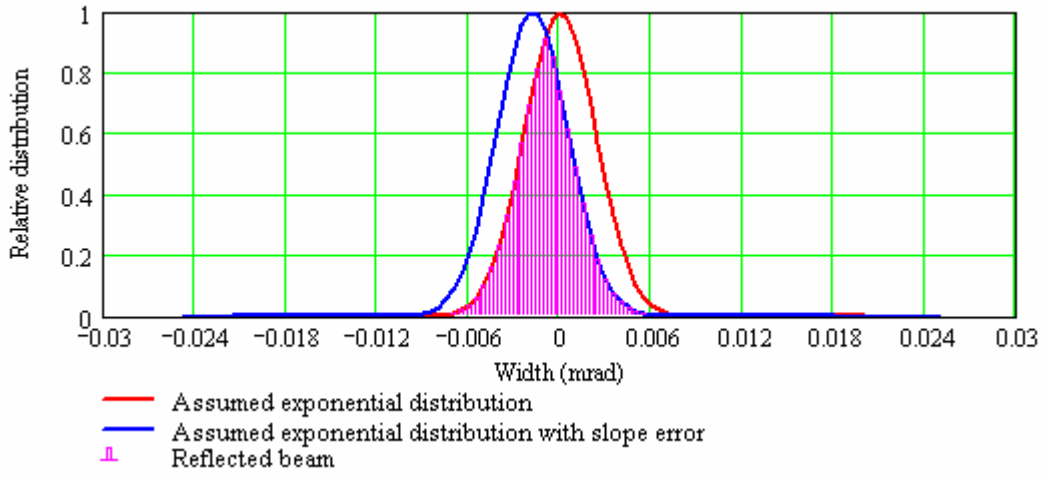

Figure 2.21 Relative distributions with slope error shift.

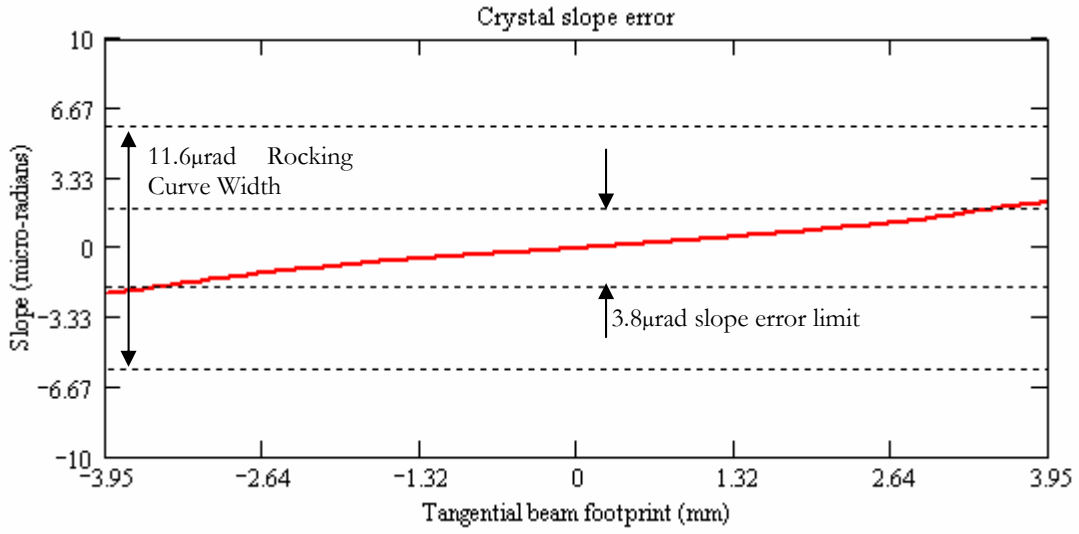

Figure 2.22 Slope profile of the first crystal with white beam incident at 24 keV.

Motion Specification. The origin for each axis will be set at the beamline source point, with the axis arrangement following the right hand rule (see Figure2.23). Some notes are provided below.

- The x-axis will be horizontal and perpendicular to the beam, in the direction away from the ring (outboard).
- The y-axis will be vertical.
- The z-axis will be horizontal and parallel with the beam, in the direction of propagation of the x-ray beam.

All rotations about a given axis are positive if, when looking along the axis in the positive direction, the rotation is clockwise.

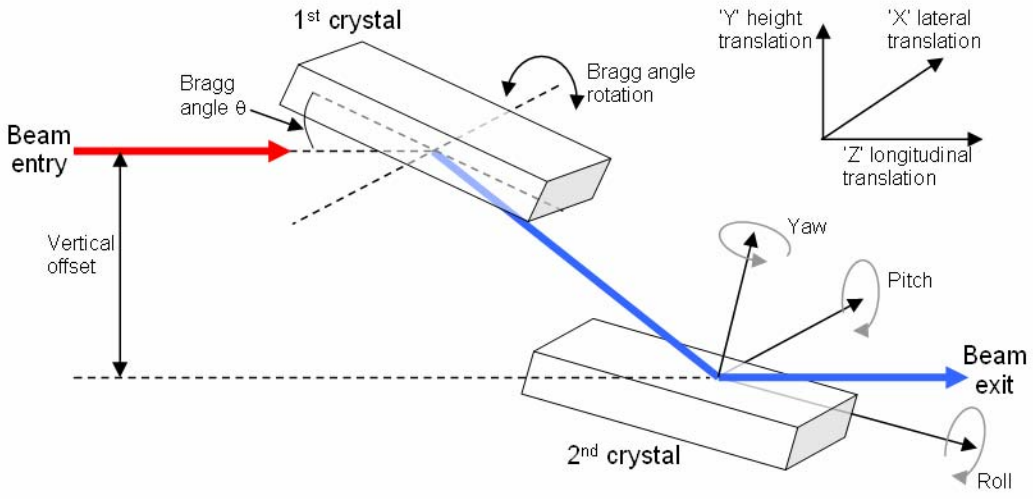

Figure 2.23 Schematic illustration of axis and angle convention.

Table 2.14 details the required motion specification for the HHLM assembly.

Table2.14 Motion Specification.

Motion	Range	Resolution	Drive system
Primary drive			
Bragg angle	-5° to 30°	<1 μrad	In vacuum stepper motor driven.
Support system			
Manual pitch (rotation about x axis)	±1°	<0.25°	System alignment.
Manual roll (rotation about y axis)	±1°	<0.25°	System alignment.
Manual yaw (rotation about z axis)	±1°	<0.25°	System alignment.
Manual lateral (x direction)	±10 mm	<250 μm	System alignment.
Manual height (y direction)	±10 mm	<250 μm	System alignment.
Manual longitudinal (z direction)	±10 mm	<250 μm	System alignment.
First crystal adjustment			
Manual roll (rotation about y axis)	±1°	<0.01°	Crystal alignment.
Manual perpendicular (Y)	±1 mm	<10 μm	Crystal alignment.
Second crystal adjustment			
Motorized coarse pitch (rotation about x axis)	±1°	<5 μrad	In vacuum stepper motor driven.
Motorized fine pitch	200 μrad	<0.05 μrad	In vacuum piezo driven.
Motorized coarse roll	±1°	<5 μrad	In vacuum stepper motor driven.
Motorized fine roll	200 μrad	<0.05 μrad	In vacuum piezo driven.
Motorized coarse yaw (rotation about z axis)	±1°	<5 μrad	In vacuum stepper motor driven.
Motorized perpendicular (to keep fixed offset)	±2 mm	<1 μm	In vacuum stepper motor driven.

2.4.3.9 White Beam Monitor (WBM)

Distance to center of undulator	30.9 m

The retractable White Beam Monitor (WBM) is a combined viewing screen and total intensity monitor for white beam (mirror in) and pink beam (mirror out), positioned directly downstream of the HHLM. It consists of a tungsten screen that is electrically isolated, water cooled, and phosphor coated. The total white and peak beam can be monitored by measuring the photo current. The beam can be visually monitored by locating a UHV window that allows a video camera to see the screen. This device will allow the position of five upstream components in succession to be optimized: 1) FEDPM, 2) FEHAM, 3) WBS, 4) HFM, and 5) HHLM. Once the alignment is complete, the WBM is retracted from the beam with a pneumatic actuator.

2.4.3.10 Bremsstrahlung Collimator (BC)

Distance to center of undulator	31.4 m

The Bremsstrahlung Collimator (BC) acts directly to restrict the size of the bremsstrahlung fan downstream. The use of external clad lead for this collimator is much less expensive than vacuum-prepared tungsten and makes best use of the limited space around this cramped area. The lead bremsstrahlung shield will comprise specially made interlocking bricks with no direct line of sight (shine path) permitted through any interspaces between the bricks. The lead will be security fastened in place to prevent removal and also will be clad in stainless steel sheet metal or Perspex covers. Connection of this standalone component is made to the beamline by flexible bellows at both entrance and exit.

The collimator is classified as a critical survey item which must not be moved once it has been set and aligned.

2.4.3.11 Monochromatic Fluorescent Screen (MFS)

Distance to center of undulator	31.9 m

The Monochromatic Fluorescent Screen (MFS) is a retractable YAG fluorescent screen that will allow the monochromatic beam to be viewed with a CCD camera for initial monochromator setup. Once the alignment is complete, the MFS is retracted from the beam with a pneumatic actuator.

2.4.3.12 Secondary Horizontal Source Aperture (SHSA)

Distance to center of undulator	32.0 m

The SHSA is an adjustable horizontal monochromatic slit intended to act as a backup secondary coherent source. The slit blades will be electrically isolated so the photo current can be measured from each blade. This will allow the SHSA to also function as a horizontal beam position monitor that can be used in a feedback mode with the HFM piezo yaw actuator.

2.4.3.13 Monochromatic Shutter (MS1)

Distance to center of undulator	32.5 m

This is a standard monochromatic shutter located close to the back wall of the optics enclosure.

2.4.3.14 Back Wall (BW)

Distance to center of undulator	33.0 m

2.4.3.15 Optics Enclosure - Incident Power Loads

Table 2.15 Summary of the Incident Heat Loads along the Optical Components within the FOE.

Component	Source Point distance	Beam size	Incident power	Transmitted power
Module 1				
Front End Differential Pump Mask (FEDPM)	14 m	1.1 mm (h) x 0.3 mm (v)		130.6 W
Front End Defining Aperture Mask (FEDAM)	1 5 m	0.3 mm (h) x 0.3 mm (v)		35.7 W
Shield Wall	26.7 m			
Module 2 Notes: Front end aperture set to 1.1 mm (h) x 0.3 mm (v)				
White Beam Filters (WBF)	27.3 m		130.6 W	
Filter thickness (μm)				
30				125.2 W
300				107.8 W
1000				87.1 W
Module 3 Note: All white beam filters removed from x-ray beam.				
White Beam Slits (WBS)	27.8 m		130.6 W	130.6 W →0 W
Module 4 Note: White beam slits open.				
Horizontal Focusing Mirror (HFM)	28.8 m		130.6 W	
reflective strip				
silicon				30.9 W
rhodium				80.7 W
Module 5 Note: Rhodium reflective strip selected on upstream mirror.				
Conductance Limiter Beryllium Window (CLBW)	29.6 m		80.7 W	75.9 W
Module 6 Note: Conductance limiter beryllium window removed from x-ray beam.				
High Heat Load Monochromator (HHLM)	30.4 m		80.7 W	0 W

2.3.6 Radiation Enclosure Design

There are several high-quality vendors for radiation hutches in Europe, as follows:

Calder-UK

Caratelli- France

Innospec-Germany

These suppliers have carried out detail design and build of radiation hutches at DLS, ESRF, SLS, and Soleil. Some of the issues the vendors need to consider are as follows:

- FOE enclosure is required to be designed as white beam enclosure.
- Stations A and B are required to be mono beam enclosures.
- The minimum shielding thickness will be in accord with NSLS-II documents.
- All the doors will be sliding doors – double for equipment and single for personnel.
- All standard enclosure heights will be 3.2 m.
- The roof of each enclosure will be surrounded by a railing to permit safe personnel access.
- Convenient access to the roof areas on the FOE, Station A, and Station B is via three access ladders.

2.4.4 Instruments

2.4.4.1 Endstation 1

Discussion of the endstation specifications and requirements is still under development.

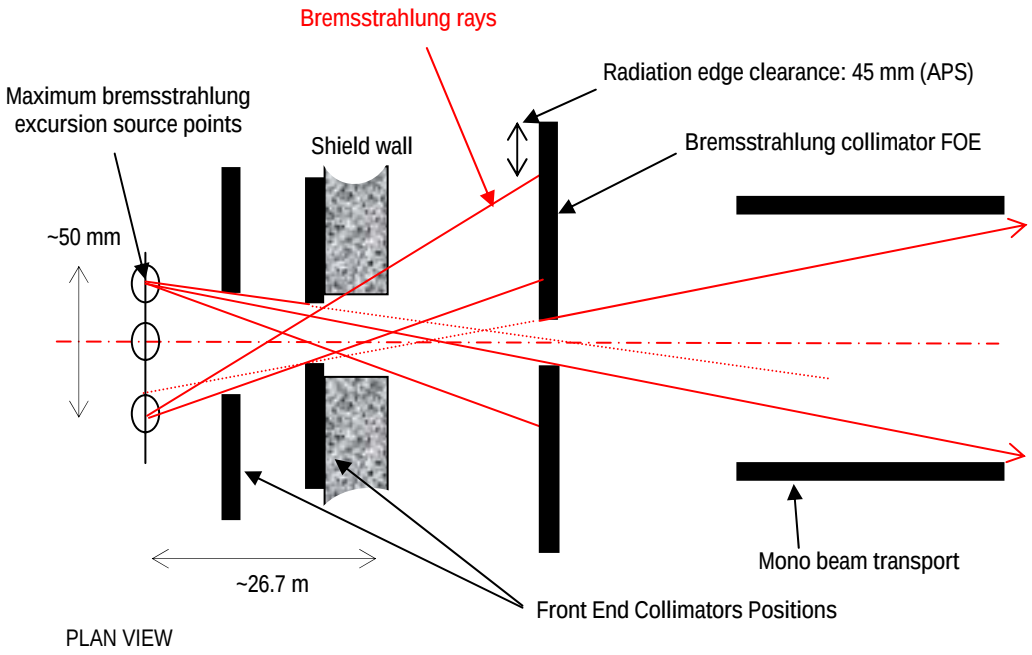

Figure 2.24. Type of bremsstrahlung anamorphic ray diagram required for effective safe beamline design.

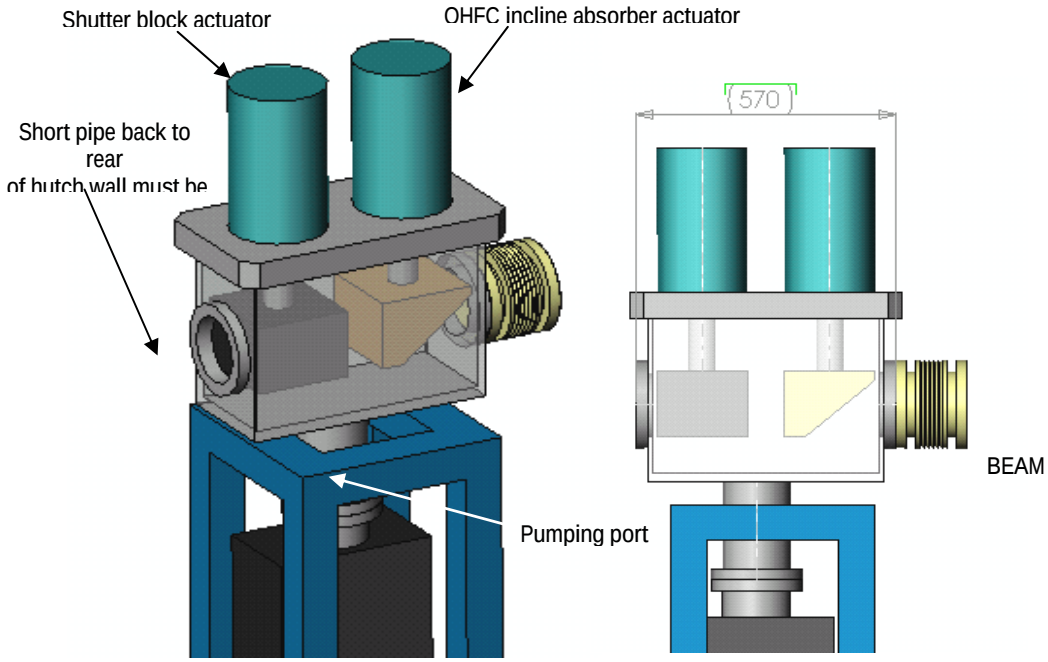

Figure 2.25 Integrated bremsstrahlung/thermal stop shutter.

2.5.3 Equipment Protection System

A Beamline Equipment Protection System (EPS) will also be required: The following table shows the preliminary fault protection logic for the beamline. The EPS protects against damage or failure due to beam heating and inadvertent vacuum let-up.

Component	Type	Action	Consequences
19-A (FOE)			
19-VALV	valve	open requested	opens valve if IMG1 ok
		close requested	closes if FE shutter closed
		air pressure fault	closes FE shutter
19-IMG01	vacuum pressure	trips high	closes FE shutter closes VALV-01 & VALV-02
19-IONP01	ion pump	on requested	turns on if IMG1 ok
19-FILT1/2/3/..	Incident Power Filter	water trips low	closes FE shutter & absorber
19-IONP02	ion pump	on requested	Turns on if IMG1 ok
19-HS1	White Beam horizontal slit	water trips low	closes FE shutter & absorber
19-VS1	White Beam vertical slit	water trips low	closes FE shutter & absorber
19-HS2	White Beam horizontal slit	water trips low	closes FE shutter & absorber
19-VS2	White Beam vertical slit	water trips low	closes FE shutter & absorber
19-VALV01	gate valve	open requested	opens valve if IMG1+IMG2 ok
		close requested	closes if FE shutter closed
		air pressure fault	closes FE shutter
19-IMG	vacuum pressure (HM mirror tank)	trips high	closes FE shutter & absorber VALV02 & 01
19-IMG	vacuum pressure	trips high	closes FE shutter closes VALV-02
19-HM	horizontal mirror	water trips low	closes FE shutter & absorber
19-IONP02	ion pump	on requested	turns on if IMG02 ok
19-VALV02	valve	open requested	opens valve if IMG2+IMG3 ok closes if FE shutter closed
		close requested air pressure fault	closes FE shutter
19-IMG	vacuum pressure	trips high	closes FE shutter closes VALV-02
19-BW1	Be window conductance limiter	water trips low	closes FE shutter & absorber
19-HHM	high heat load monochromator	water trips low	closes FE shutter & absorber
19-IONP04	Ion pump	on requested	Turns on is IMG03 ok
19-WBM	white beam monitor	LN2 trips low	closes FE shutter & absorber
19-STOP1	bremsstrahlung stop	Fixed item Possibly water cooled stop- water trips low	FIXED aperture closes FE shutter & absorber
19-MFS1	monochromatic fluorescent screen	water trips low	closes FE shutter & absorber
19-VALV03	valve	open requested close requested air pressure fault	opens valve if IMG3+IMG4 ok closes if FE shutter closed closes FE shutter
19-IMG04	vacuum pressure	trips high	closes FE shutter closes VALV-03

Component	Type	Action	Consequences
19-SHSA	secondary horizontal source aperture	water trips low	closes FE shutter & absorber
19-IONP05	ion pump	on requested	turns on if IMG04 ok
19-SHUTTER1	monochromatic shutter	open (thru) requested close (stop) requested	opens 19-FE shutter closes 19-FE shutter
19-FOE	back wall for FOE (ID-A)	trips high	closes FE shutter & absorber closes VALV03
19-SBT1	shielded beam transport	on requested	turns on if IMG ok
19-	front wall of hutch (ID-B)		
19-VALV04	valve	open requested close requested air pressure fault	opens valve if IMG4+IMG5 ok closes if FE shutter closed closes FE shutter
19-IMG	vacuum pressure	trips high	closes FE shutter closes VALV-04
19-QDBPM	quad diode BPM		
19-THSA	tertiary horizontal source aperture		
19-IONP	ion pump	on requested	turns on if IMG ok
19-MFS2	monochromatic fluorescent screen		
19-VALV05	valve	open requested close requested air pressure fault	opens valve if IMG5+IMG6 ok closes if FE shutter closed closes FE shutter
19-IMG06	vacuum pressure	trips high	closes FE shutter & absorber closes VALV05
19-IONP07	ion pump	on requested	turns on if IMG06 ok
19-HRM	high-resolution monochromator		
19-BW2	Be window		
19-NFO1	nanometer focusing optics		
19-	back wall of (ID-B)		
19-SBT2	shielded beam transport		
19-	front wall of (ID-C)		
19-NFO2	nanometer focusing optics		

Notes: Vacuum pressure trips using Inverted Magnetron Gauges (IMG) and not Piranis on each gauge cluster

Figure 2.26 is a diagram of the vacuum flow for the HXN beamline. Figure 2.27 is the EPS diagram.

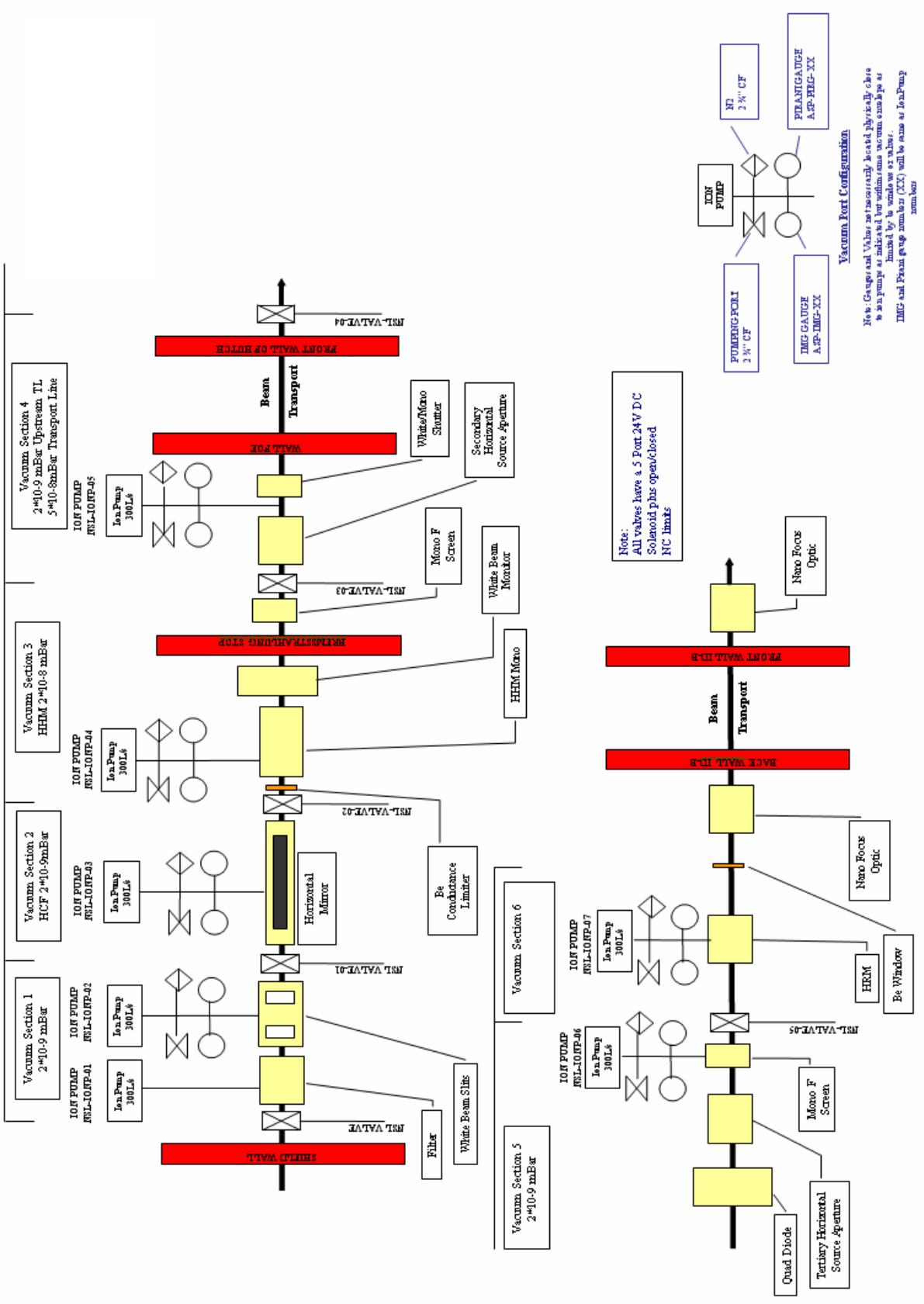

Figure 2.26 Hard X-ray Nanoprobe Beamline Vacuum Flow Diagram

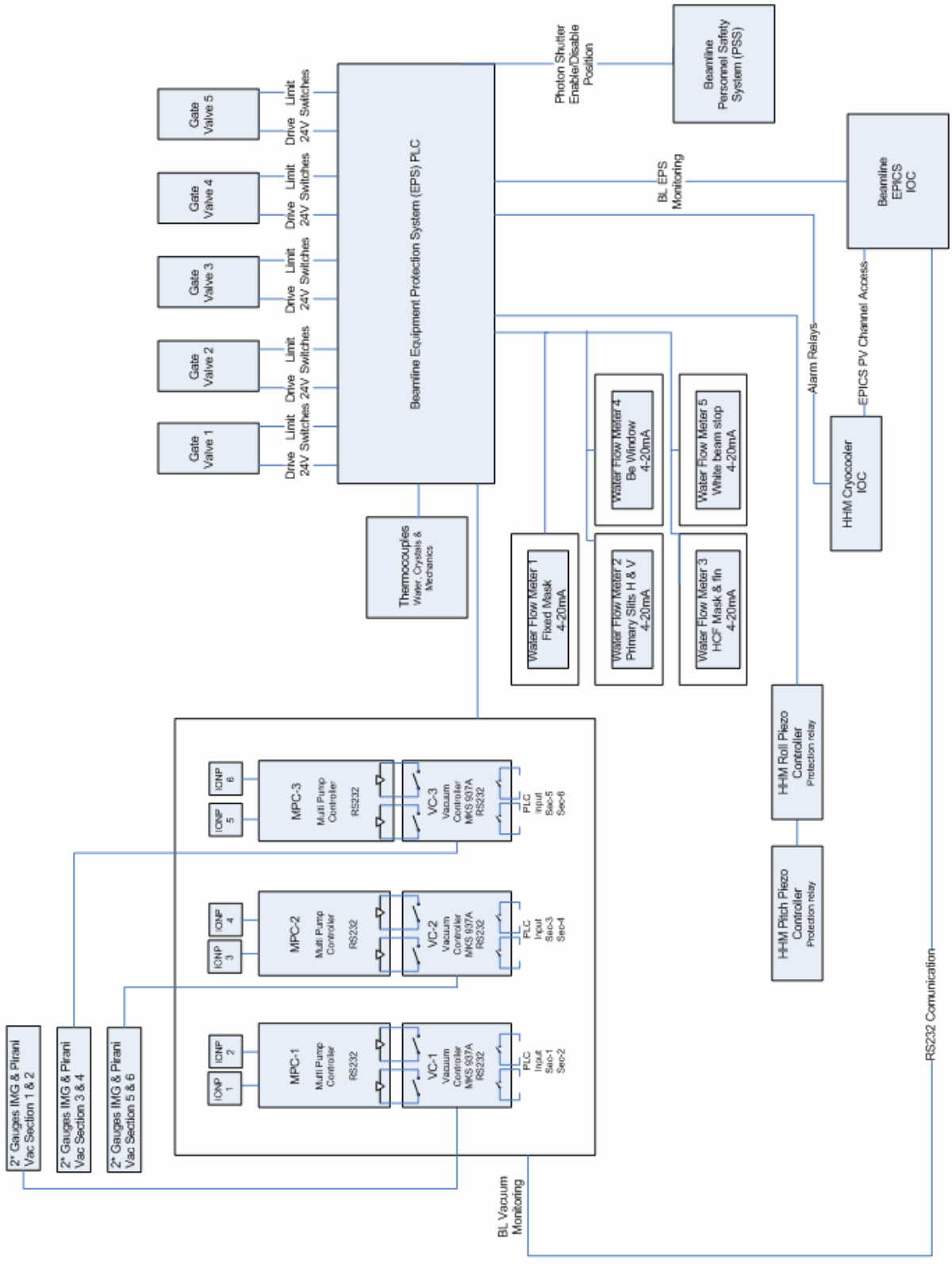

Figure 2.27. EPS Diagram.

2.6 Additional Requirements Imposed on the Conventional Facilities

2.6.1 Vibration Considerations for Synchrotron Beamlines

The beamline vibration is a mammoth subject which ranges from the influence of the distance ocean waves to the local structural resonance. This short discussion has been split in to two sections. The first section addresses vibration sources and the second section presents good engineering design practices.

2.6.1.1 Vibration Sources

Prior to beamline installation it is advisable to characterize the local experimental floor slab. The ambient displacement spectrum will be measured for an extended period of time (>24 h) to increase the likely hood that infrequent vibration sources are observed. NSLS-II should have a sitewide vibration log,, but local structures can affect the results. An example of such a case was a deformed slab at ESRF which, due to the reduced ground contact, increased the displacement amplitude by a factor of 10. The problem was resolved by the injection of grout into the interface.

The vibration source spectrum may be split into three conceptual regions, low-, medium-, and high-frequency. The sources that generate frequencies below 1 Hz (low frequency) tend to be seismic activity, ocean waves, and thermal expansion. The medium-range frequencies (1 – 100 Hz) are generated by machines, pumps, traffic, fluid flow, and mechanical resonances. The high-range (>100 Hz) frequencies are often acoustic, electro-mechanical, and well-designed mechanical resonances.

A proactive approach must be employed when addressing the vibration influence on a beamline. The low-frequency vibration amplitude will be dominated by the quality of the experimental floor and the air conditioning. The associated electron beam and x-ray beam motions may be effectively compensated by the use of closed-loop control systems on the steering magnets and mirrors. The medium-frequency mechanical sources of vibration, such as water chillers or vacuum pumps, should be identified, then moved or isolated. Care must be taken to consider even non beamline components, such as the insertion device (ID) cryostat, or automotive traffic vibrations, which may even be reduced by the removal of speed bumps and drain covers, for example. An instance of a high-frequency vibration source is an optic actuator and the respective support structure stiffness. These effects may often be reduced by the choice of good-quality drive electronics and electrical ground.

2.5.1.2 Good Engineering Design Practices

A wide range of engineering design practices have been empirically developed for synchrotron vibration management. The most basic concept is that only relative motion between the beam and the sample will be detrimental, so all the optics must be mounted from a monolithic floor slab. The most critical components are the mirrors and monochromator. The optical lever arm greatly amplifies vibration effects.

The most common form of vibration isolation within industry is the damping/isolation pad; however, the inherent position instability introduced by an elastic support element can introduce undesirable long-term position drift. For this reason, the optics are usually mounted on stiff supports that are mechanically isolated from their surroundings. Optics are usually mounted on top of a natural or synthetic granite block of high mass and low natural frequency. Granite has good vibration damping properties and a lower thermal expansion coefficient than steel fabrications. The stiffness of the granite may be increased by grouting the block to the floor, although this is often avoided for practical reasons. The upper optic assembly is then designed to be stiff with a high fundamental resonant frequency. Vibration mode analysis and FEA may be used to optimize the design. A high resonant frequency is desirable, as it is less likely to coincide with driving vibration sources and also requires more energy to be driven.

It is possible to extend the high-resonant-frequency philosophy down to the floor. Good results have been achieved using a bolted, lightweight, large cross-section metal structure instead of a massive block. The light

weight and large cross section increase the resonant frequency and the bolted interfaces provide vibration damping.

A number of methods can improve existing mechanical systems, such as the addition of external viscoelastic damping links, which take no mechanical load or tuned dampers.

A closed loop beam stabilization system is commonly employed to effectively lock the beam spot on to the sample position. The signal from a beam position monitor (BPM) is used to drive an upstream mirror or monochromator to compensate for any relative motion via a PID loop. The effectiveness of a closed-loop beam position system to remove vibration reduces as the detrimental frequency rises. In general, the greater the feedback loop frequency the higher the threshold for vibration compensation. A high-frequency, closed-loop beam position system typically runs at ~1 kHz.

It is possible to tune some unavoidable vibration sources to reduce their effect on the beam position. The pump speed and pressure of cryo-coolers may be adjusted to minimize beam influence. Software notch filters may be added to the motion control system to avoid known resonant frequencies.

In summary, vibration will be considered at each stage of beamline design installation and commissioning.

2.6.1.3 Choosing an Optical Top or Breadboard

The broadband damping characteristics are possibly the most important table specification to consider. Tables may employ tuned damping systems; however, these will become invalid as the load mass and location change. The broadband damping may be achieved with oil-based systems or solid dampers. The solid option is preferable, because oil characteristics can change over time and there is the possibility of an oil reservoir being pierced.

The current state-of-the-art system is the TMC Maximum Dry Damping, the performance of which is presented below. TMC offer their leading technology in a range of sizes, all using CleanTop II technology, which insures that fluids are not able to enter the table interior.

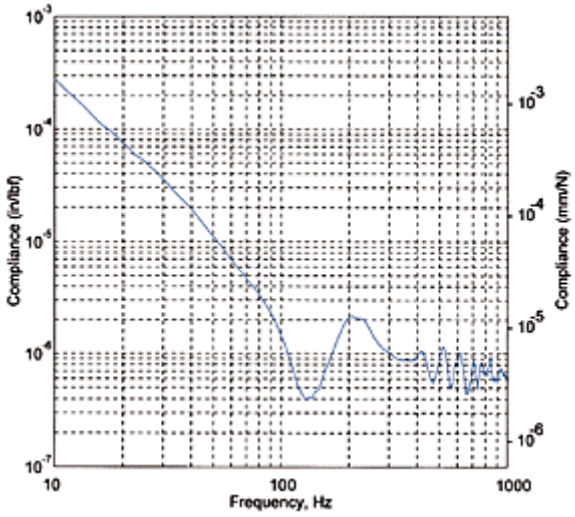

The TMC optical table top can be combined with their cutting edge STACIS active vibration cancellation system. The STACIS system provides a stiff mounting system that effectively reduces vibration in the range from 0.6 – 250 Hz. It was designed for precision microlithography and metrology. Example performance curves are given below.

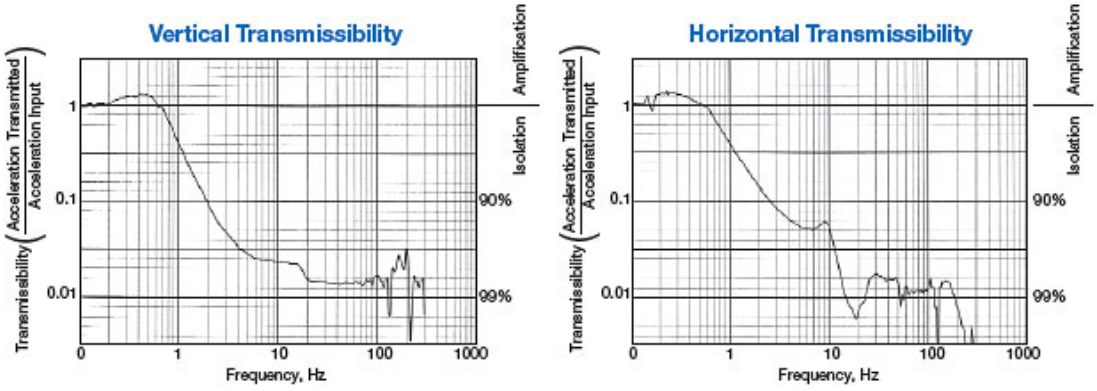

2.7 Additional Requirements Imposed on the Accelerator Systems

The current stability goals for the accelerator performance are sufficient for this beamline.

References

1 K. J. Kim, Angular Distribution of Undulator Power for an Arbitrary Deflection Parameter K, *Nuclear Instruments and Methods in Physics Research,* A246 (1986) 67-70.

2 *LS 237: Explosion Bonding of Dissimilar Materials for Fabricationg APS Front End Components—Analysis of Metallurgical and Mechanical Properties and UHV Applications,* Yuheng Li, Deming Shu, and Tuncer M. Kuzay, Experimental Facilities Division.

3 D. Shu et al. (1995). Precision white-beam a list design for high power density x-ray undulator beamlines at the APS. *Rev. Sci. Instr* **66**(2) Feb 1995.

4 M. Rivers et al. GSECARS Report, First Results from the Sector 13 (GSECARS) Undulator Beamline.

5 B. Fell, K. Fayz, Experimental Investigation of Thermal Contact Resistance for Indirectly Cooled SR Optics, MEDSI 2000.

6 Cryogenic cooling monochromators for SPring-8 undulator beamlines, *Nuclear Instruments and Methods in Physics Research A 467-468 (2001) 647-649.*

2-A Appendix A: Optical Study

2.A.1 Optics Overview

This section presents an overview of the proposed optics plan. It follows the ideas presented in the December 2006 NSLS-II CDR and suggests additional modes. Determining an optics plan for this beamline is complicated by the fact that the required final optics for achieving 1 nm do not yet exist. The uncertainty associated with the optics requires that the beamline be designed with sufficient flexibility to provide the necessary contingency to accommodate an eventual optics solution. The challenge is to provide this flexibly without paying an excessive cost premium or the need to rebuild / replace components, allowing on budget and on time completion of the beamline. The following optics plan incorporates this flexibly and controls risk by utilizing well understood front end and FOE optics components to deliver the x-ray beams generally required for illuminating any successful nano-focusing optics.

The plan is based on two focal points – one at 41 m and the other at 76 m – both supplied by a common set of upstream optics located in the front end and FOE. At each of these two locations a hutch would be constructed that is capable of housing the necessary end station equipment to support the scientific goals of the beamline. The exact location of these hutches will be determined by a number of factors such as the characteristics of the final nano-focusing optics and details involving conventional facilities (floor space, roof line, egress, utilities, etc.). One way to look at this proposed layout is to consider the 41 m hutch a 1x location and the 76m hutch a 2x location with regard to beam demagnification. Operationally, the focused x-ray beam can be used in only one hutch at a time. A beam stop located at the back wall of the upstream 1x hutch would provide access to the downstream 2x hutch while beam is present in the 1x hutch. Access to the 2x experimental location during x-ray operation of the 1x location will allow off line work to be performed using the end station equipment. Given the sophistication and complexity of a nanoprobe end station, this will provide valuable access time for instrumentation development and debugging as well as experiment setup.

The 1x/2x hutch arrangement will play a key role during the early operation phase of the project when the main activity will be optics testing and commissioning. During this initial phase and well before the 2x hutch (and transport to it) is completed, the 1x location will serve as an early test sight where various optics approaches can be evaluated and refined for eventual use in the push to 1 nm in the 2x hutch. There also exists the possibly of achieving a 1nm focal spot at the 1x location if modes such as a wave guide coupled aperture prove feasible. The two locations can also be instrumented with complimentary end station equipment such as a full-field imaging system in the 1x location providing flexibly and agility in meeting the demands of the user science program.

Below, five optics modes are presented – two for the 76m 2x location and three for the 41m 1x location. The five modes are:

- direct focusing at 76 m
- compound horizontal focusing at 76 m
- waveguide mode at 41 m
- direct mode at 41 m
- compound horizontal KB focusing mode for full-field imaging at 41 m.

The proposed support optics will be used to configure these five modes and are general enough to provide additional operation modes if necessary. They are also well understood today regarding both performance and cost. The order of presentation in this document follows the flow of the x-rays from the storage ring to the sample. The components common to all five modes will be presented first followed by discussion of each mode.

2.A.2 Critical Optics Components

In this section we discuss only optical components of primary importance to the five operation modes. For a complete component description of the please see full beamline description.

2.A.2.1 Storage ring and Insertion Devices

The first optical component to be considered in a beamline plan is the storage ring and insertion device. For this report we used the source parameters found in the NSLS-II July 2007 user workshop report. The values used are listed in Table 2.A.1 for a low-beta straight. The NSLS-II U19, 3m long undulator is an excellent source of hard x-rays. It has the advantage of effectively utilizing the storage ring's brilliance and producing hard x-rays from 2 to 30 keV that are well matched to the required optics.

2.A.2.2 Front End Fixed Mask (FEFM) and Differential Pump (DP)

This power limiting mask will allow approximately 90% of the undulator harmonic (at 1 Å) to pass, reduces the total power to a level that is more manageable by the downstream components and protects against miss-steered of the electron beam. It will be located behind the shield wall as close to the undulator as possible (~14 m) with the next component (horizontal source aperture) directly downstream. The vertical and horizontal location of this critical component will be defined through survey with additional motorized horizontal positioning over a restricted range to aide the initial alignment of the orbit (its front end location will make it difficult to access manual adjustors.) Due to its location and size this component is ideal for acting as the vacuum conduction limiting aperture for a differential pump, freeing up space in the FOE. See power management report section for thermal performance analysis.

2.A.2.3 Front End Adjustable Horizontal Source Aperture (FEHA)

This adjustable horizontal mask at ~ 14.5 m will allow the horizontal beam size to be restricted to match the effective vertical coherent source size during nano-focusing. The aperture can be opened to match the FEFM horizontal size for full-field operation mode. The aperture will be constructed as two wedges with one motor adjusting the aperture size and the other it's horizontal position. See power management report section for thermal performance analysis.

2.A.2.4 Horizontal Focusing Mirror (HFM)

This will be a flat horizontally deflecting mirror located at 28.8 m used for power management and as a horizontal focusing element for compound horizontal focusing modes. It will be water cooled with a two moment bender. The mechanical bender will allow the mirror figure to be corrected for thermal bump when producing unfocused beams as well as allow the horizontal beam to focused either directly onto the sample or over a ranged of secondary horizontal source locations from 3.2 to 9 m, resulting in demagnifications from 9 to 3.3. In compound horizontal KB focusing mode for full-field imaging at 41m nearly the full horizontal source can be collected and focused onto the sample using this mirror. The mirror will be fabricated from silicon have an active length of approximately 600 mm, coated over ½ its width with Rh and operate from 0 – 3 mrad. At its maximum incidence angle (3 mrad) working off the Rh stripe it will have an entrance aperture of 1.8 mm with an energy cut off of approximately 20 keV and capable of collecting 89% of the full horizontal undulator source. With a ½ Rh coating the bare silicon stripe can be used to achieve higher harmonic rejection for low energy operation.

Table 2.A.1 Source Parameters from NSLS-II July 2007 User Workshop.

	Based on July 2007 Workshop
Electron Energy	$E = 3GeV$
Stored Current	$I = 500\ mA$
Electron Beam Emittance	
Horizontal	$\varepsilon_x = 0.55\times10^{-9}\, m-rad$
Vertical (1.5% Coupling)	$\varepsilon_y = 8.25\times10^{-12}\, m-rad$
Betatron Function§	
Horizontal	$\beta_x = 1.5m$
Vertical	$\beta_y = 0.8m$
Electron Beam Size§	
Horizontal	$\sigma_x = 28.7\mu m$
Vertical	$\sigma_y = 2.57\mu m$
Electron Beam Divergence§	
Horizontal	$\sigma_x^{'} = 19.2\mu rad$
Vertical	$\sigma_y^{'} = 3.21\mu rad$
Intrinsic Photon Size*	$\sigma_r = 1.95\mu m$
Intrinsic Photon Divergence*	$\sigma_r^{'} = 4.08\mu rad$
Total Photon Source Size§*	
Horizontal	$\sum_x = 28.8\mu m$
Vertical	$\sum_y = 3.2\mu m$
Total Photon Source Divergence§*	
Horizontal	$\sum_x^{'} = 19.6\mu rad$
Vertical	$\sum_y^{'} = 5.19\mu rad$

§ = Low b straight.

*Quantities evaluated for 12.4 keV x-rays and a 3m long undulator.

2.A.2.5 High Heatload Monochromator (HHM)

This will be the primary monochromator on the beamline located at approximate 30.4 m, with LN2 cooled Si 111 crystals operating with a fixed offset of 20 mm over an energy range of 4 – 24 keV. The fixed offset will be maintained by allowing the gap between the faces of the first and second crystal to change (range of motion < 1.5 mm) and the beam to walk along the surface of a long (115 mm) second crystal. Eliminating the

"z-stage" on the second crystal and replacing it with a long crystal greatly improves ease of tuning energy as well as stability since the second crystal is more rigidly mounted. Thermal and vibration stability will be of primary importance in this monochromator design. The direct LN2 cooling needed to maintain the thermal distortions at acceptable levels has the potential for introducing unacceptable vibration. Managing vibration issues at the level suitable for a nano focus beamline will require R&D effort and prototypes resulting in additional cost. See power management report section for thermal performance analysis.

2.A.2.6 Secondary Horizontal Source Aperture (SHSA) + BPM

This is a high quality monochromatic aperture located at 32 m and adjustable horizontal. It will provide a secondary horizontal coherent source as well as a horizontal beam position monitor that can be used in a feedback mode with the HFM PZT pitch actuator. It will be of a relative open and center position type. The blades will be electrically isolated so that the photo current can be measured from each blade.

2.A.2.7 Quad Diode BPM (QDBPM)

This device located at 37.5 m and just inside the upstream wall of the 1 x experimental hutch. For this device the x-ray beam is incident on the face of a 1 micron thick foil generating x-ray florescence that is collected by vertical and horizontal pairs of diodes. As the beam moves on the face of the foil the solid angle of the florescence intercepted by each diode changes. The beam position is determined by computing the difference over the sum of the diode pairs. The foils are mounted on a filter wheel with six positions (one left empty) so that foil with an edge close to the beam energy can be used. Since both vertical and horizontal position information is available this device can be used in a closed loop feedback mode with the PZT's (pitch and roll) of the monochromator and or the horizontal mirror pitch PZT. This closed loop feedback can be used to stabilize the beam position. The QDBPM will be mounted on a vertical translation stage supported off the same structure as the tertiary horizontal source aperture (THSA) – see next item.

2.A.2.8 Tertiary Horizontal Source Aperture (THSA)

This is a high quality aperture located at 37.8 m that will be used to control the size of the horizontal source image produced by the HFM when operating in horizontal compound focusing mode. It will be of a relative width and center slit type with sufficient range to follow the horizontal deflected beam.

2.A.2.9 High-Resolution Monochromator (HRM)

The high-resolution monochromator located at 39 m will operate in a back scatter geometry (first crystal downstream of the second crystal) to achieve the energy resolution required for nanometer size beams. It will consist of diamond 111 crystals allowing use of higher order reflections to cover the required energy range. The crystals will be mounted on a water cooled heater stage held at constant temperature using feedback. Each crystal will be mounted on an independent high-resolution rotation stage. The first crystal rotation stage will be fixed and the second will be free to travel on a z stage so that the monochromator can be operated in fixed offset mode.

2.A.3 Optics Modes

In this section we present an analysis of five optics mode. Common to each mode is a working distance of 10 mm. A working distance of 10 mm or less is most likely needed to reach a 1nm goal. Such short working distances will severely limit the space available for items such as detectors and sample viewing optics and will require that the final focusing optic (i.e., MLL, Kinoform lenses) support structure be optimized to reduce their transverse size. Setting the working distance goal as long as 10 mm provides a safety factor should higher demagnifications be required.

The ray trace analysis presented here were conducted using a program written in IDL at the University of Chicago Center for Advanced Radiation Sources that is optimized for large and small KB optics and capable of optimally figuring both straight and tapered mirrors through the application of upstream and downstream moments. All ray-tracing is performed using realistic mirror shapes and in the case of the small KB mirrors the well established approach (see Eng et al. SPIE Proc. 3449, 145 (1998)) of dynamically figuring the mirror shape by applying two adjustable moments to a trapezoidal shaped mirror is used.

2.A.3.1 Direct Focusing at 76 m

Figure 2.A.1 shows the vertical and horizontal optics layout for the direct focusing mode at 76 m. The inserts shows scatter plots of ray traces of the source at the front end aperture and at the location of the final focusing optics. The location of the final focusing optics is defined simply by the 7.6 μm FWHM vertical source size, the 10 mm working distance, and the desired 1 nm beam size. In addition to the final focusing optics, the only other components required are the front end aperture and high-resolution monochromator. The transverse coherence angle of the vertical source at 1 Å is 6.6 μrad and is achievable with a vertical aperture at 14.5 m of 120 μm, resulting in a vertical optical aperture at 76 m of 500 μm.

In the horizontal dimension, the source is nearly 10 times larger. In order to match the vertical focus, the horizontal size of the front end aperture must be 10 μm or less. The divergence through such an aperture is defined by the size of the horizontal source and the distance to the aperture and is approximately 5 μrad. This matches well the transverse coherence angle of the new horizontal source, defined by this aperture as 5.5 μrad, resulting in a horizontal optical aperture at 76 m that is well matched to the vertical.

The scatter plots in A.2.A to the left of the front end aperture show the full beam available from the undulator. The top panel is a plot of the vertical and horizontal source, with the missing center rectangle indicating the portion of the beam that can be used by the final focusing optics. The lower panel shows a phase space plot in the horizontal direction with the vertical white band showing the portion of horizontal phase space used by the final focusing optics. To the right of the aperture are the same plots, but they now show just the transmitted beam. Figure A.x.x shows a detail view of the source that illuminates the final focusing optics, where a little less then 1% of the total undulator beam is accepted.

2.A.3.2 Compound Horizontal Focusing at 76 m

In the compound horizontal focusing mode at 76 m the horizontal focusing mirror located at 28.8 m is used to produce a secondary horizontal source at 32 m. In this mode the vertical optics are identical mode discussed above. The horizontal optics layout and ray trace scatter plots are shown in Figure A.2.x. This horizontal mirror geometry results in a horizontal demag = 9 and produces a horizontal focus with a FWHM of 7.6 μm. To be able to achieve a 1nm horizontal focus, this secondary source must be reduced to 4 μm using the secondary source aperture. The divergence of this secondary source in very large (~0.5 mrad), and the horizontal transverse coherence angle of this source is about 11 μm, requiring that nearly a factor of 50 of the full divergence be masked out of the beam that illuminates the final focusing optics. The scatter plots at the secondary source aperture show full and the masked secondary source. The scatter plots at 76 m show the beam that will illuminate the final focusing optics, showing that approximately 1 % of the total undulator beam can be made available to the optics.

One possible advantage of this mode is that the horizontal source size can be tuned by adjusting the secondary source slit. An additional advantage is that the secondary horizontal source could be stabilized on the secondary source aperture, using a feedback loop that adjusts the pitch of the horizontal mirror.

2.A.3.3 Waveguide Mode at 41 m

Figure A.2.4 shows the waveguide mode used at 41 m. In this mode primary focusing optics with a working distance of 30 mm and an aperture of 269 μm would produce a secondary source that is 50 μm FWHM. This source is then coupled to an x-ray wave guide. The waveguide will pass only a coherent source and will act as a secondary source for the secondary focusing optics. A demagnification of only 50 is now needed to achieve 1 nm focus. The secondary focusing optics would have an optical aperture of 500 μm and a working distance of 10 mm.

2.A.3.4 Direct Mode at 41 m

The direct focusing mode at 41 m is the same concept as the direct mode at 76 m. The final focusing optics would have a demagnification of 4133 and an optical aperture of 273 μm and would focus the beam to 1.89 nm at a working distance of 10 mm.

2.A.3.5 Compound Horizontal KB Focusing Mode for Full-Field Imaging at 41 m

Full-field imaging greatly benefits from the high photon flux, divergence, and small spot size produced using the compound horizontal small KB focusing mode. Figure A.2.x and Figure A.2.x show the horizontal and vertical optics layout respectively. In this mode the horizontal focusing mirror at 28.8 would focus the beam 9 m away at the tertiary horizontal aperture with a demagnification of 3.3. The horizontal beam size at this aperture is 51 μm FWHM and is re-imaged by a small KB mirror located 3.33 m away. This small KB mirror with a demagnification of 16 and a working distance of 90 mm produces a final focus of 1.4 μm FWHM. In the vertical (Figure A.2.x), only a single small KB mirror is used with a demagnification of 91, producing a vertical focus of 92 nm FWHM. The first two scatter plots in Figure A.2.x show the tertiary focal spot with the aperture fully open and set to 2 μm. The third and fourth scatter plot show the final focus produced by the small KB mirror pair for the case the tertiary aperture fully open and closed to 2 μm, resulting in a horizontal focus that ranges between 1.4 to 0.1 μm FWHM and transmitting 69% to 6% of the undulator source.

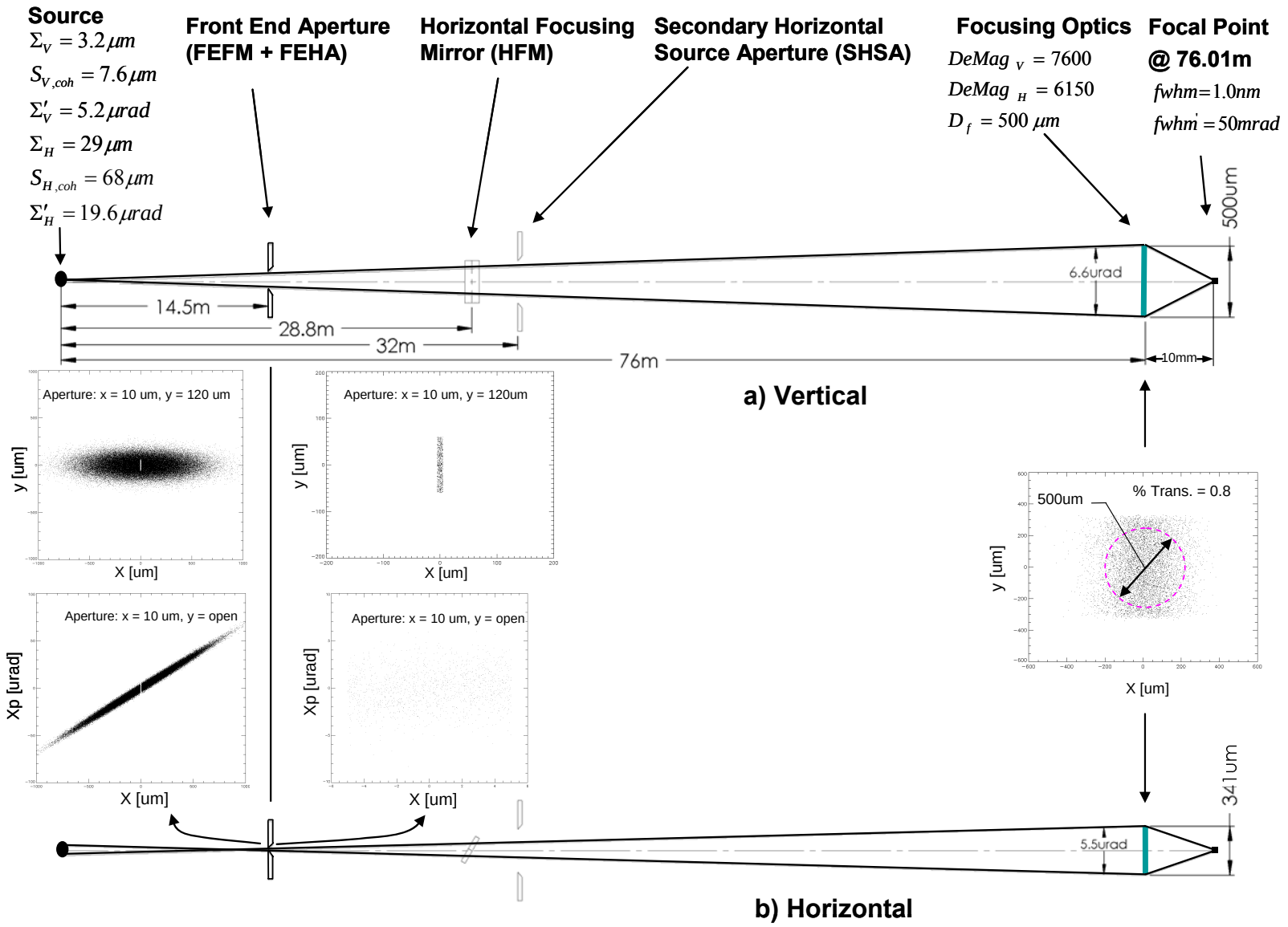

Figure 2.A.1. Optics layout and ray trace for a direct focusing at 76 m, focusing the beam to 1 nm with a working distance of 10 mm. a) vertical ray trace, b) horizontal ray trace.

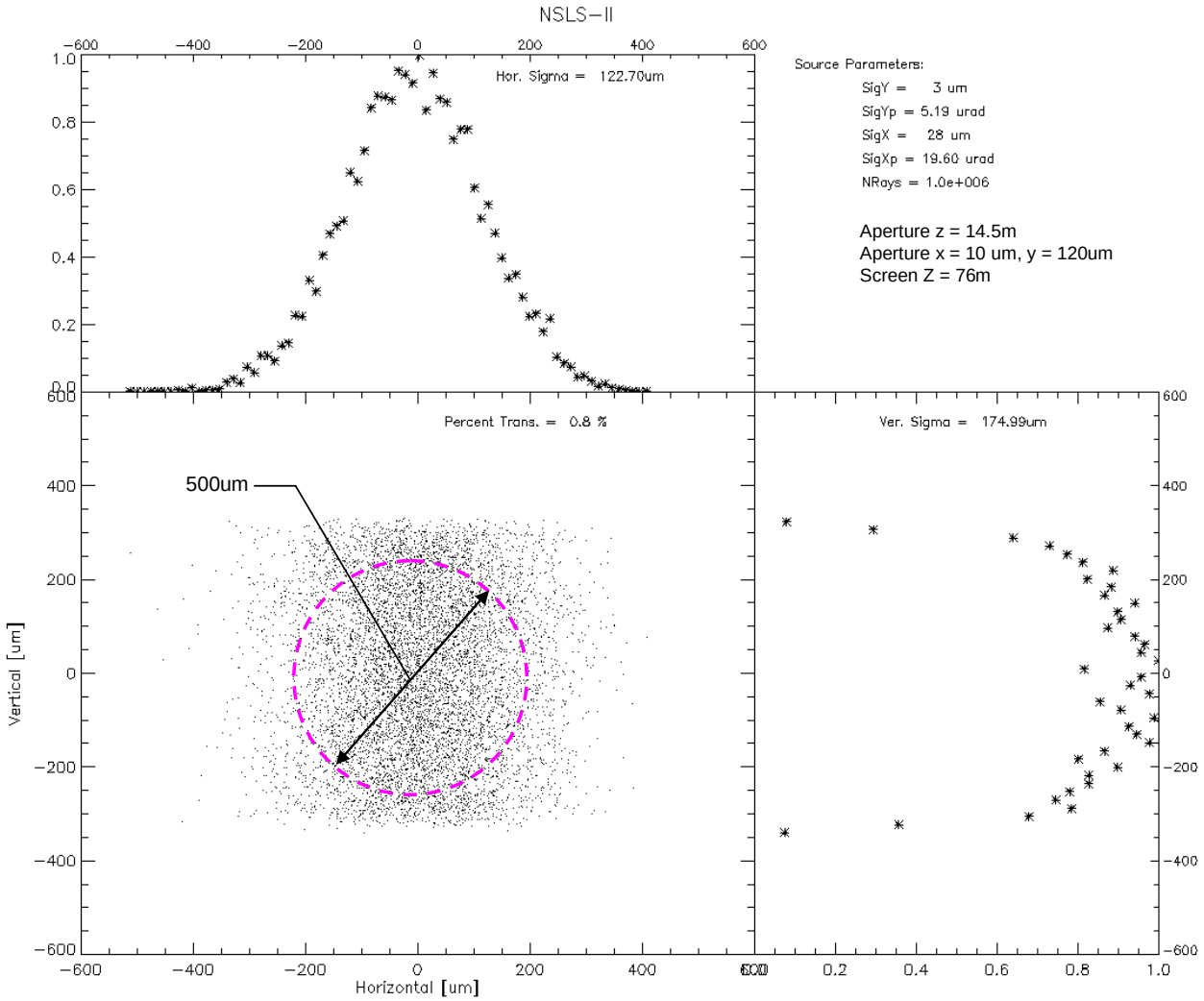

Figure 2.A.2. Scatter plot of coherent beam illuminating the nano-focusing optics for direct focusing at 76 m. 0.8 % of the total undulator harmonic is transmitted to the final optic.

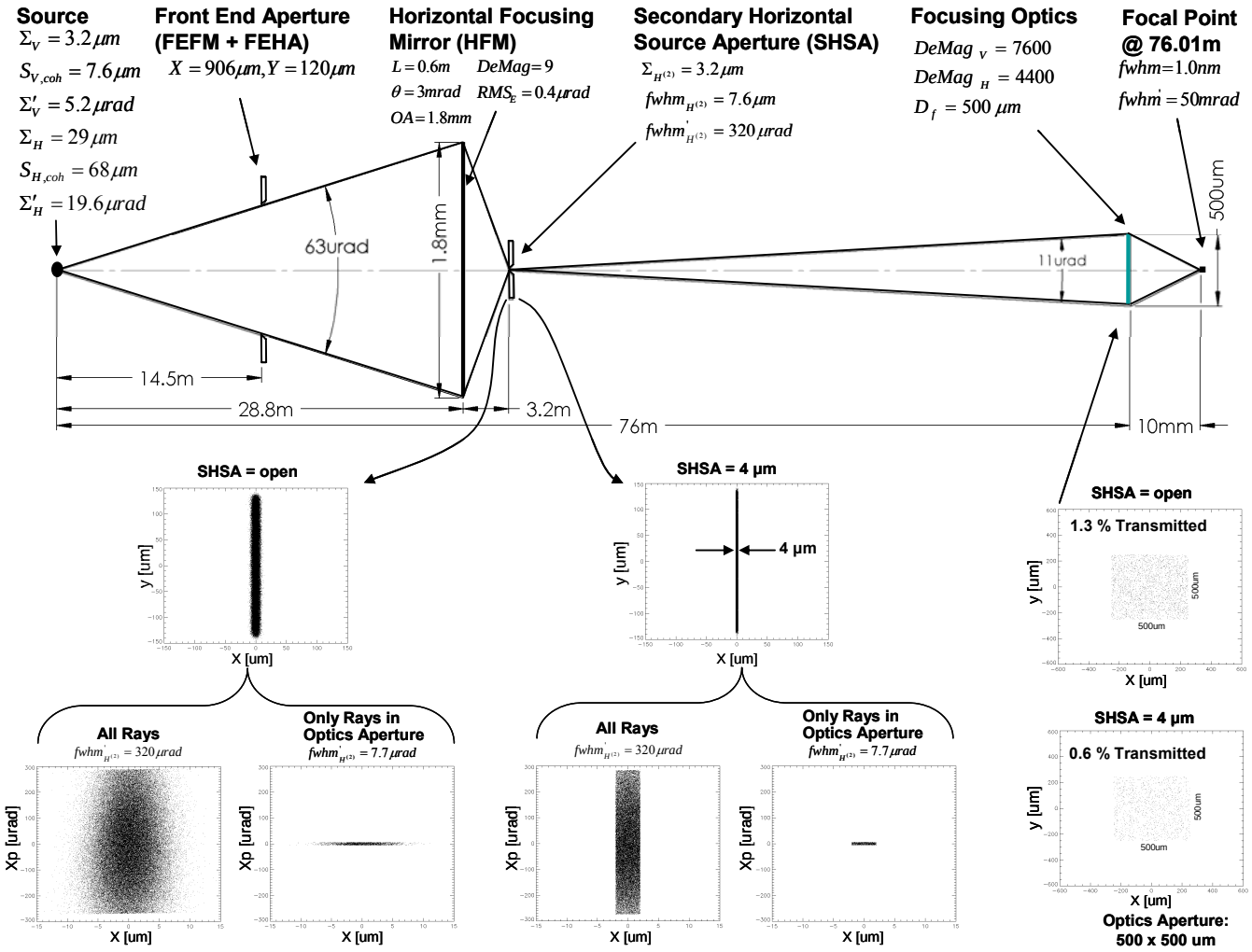

Figure 2.A.3. Optics layout and ray trace for a compound horizontal focusing at 76 m, focusing the beam to 1 nm with a working distance of 10 mm.

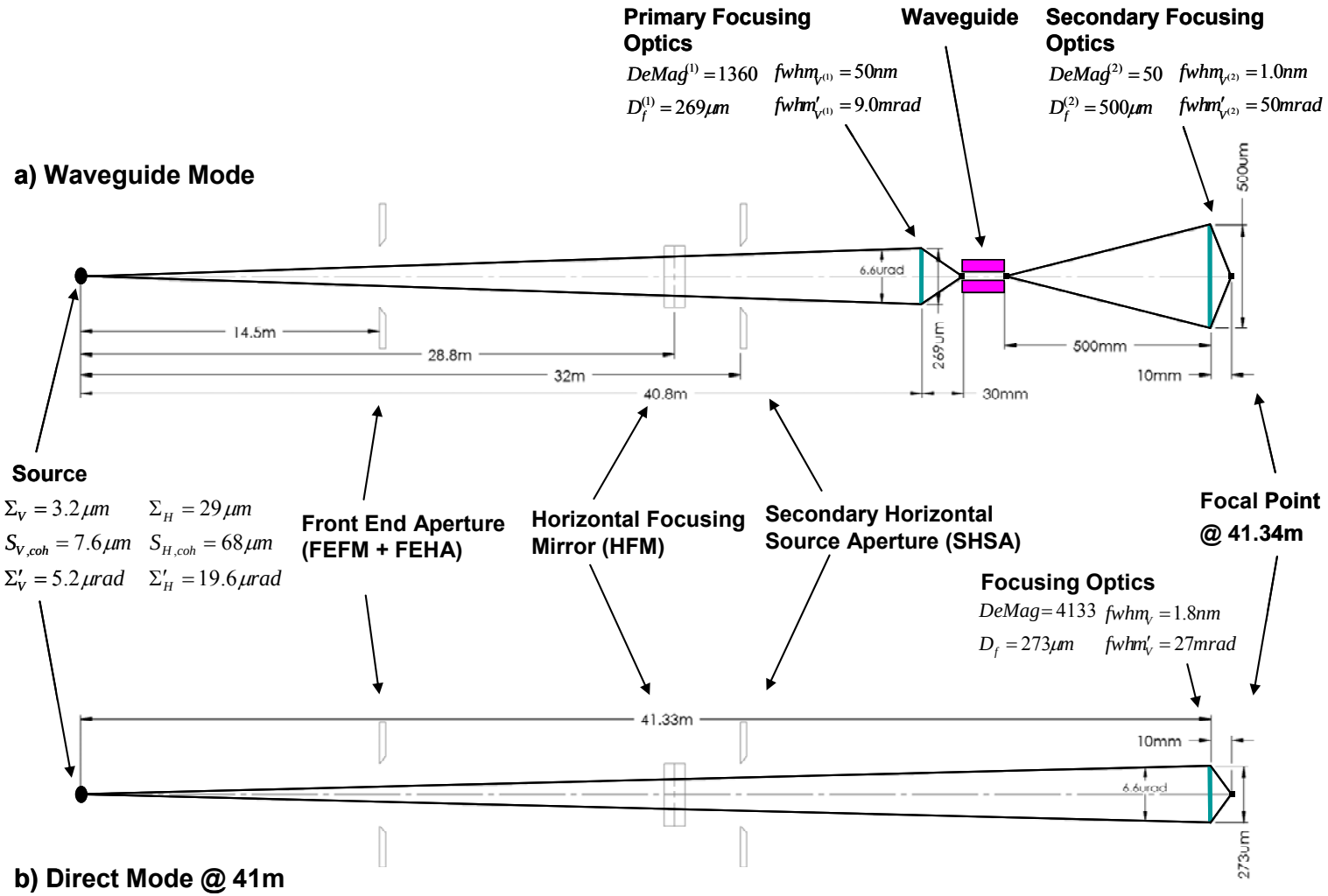

Figure 2.A.4. Optics layout for focusing at 41 m. a) Waveguide mode achieving 1 nm at 41 m with a working distance of 10 mm. b) Direct beam mode with the beam focused to 1.8 nm at 41 m with a working distance of 10 mm.

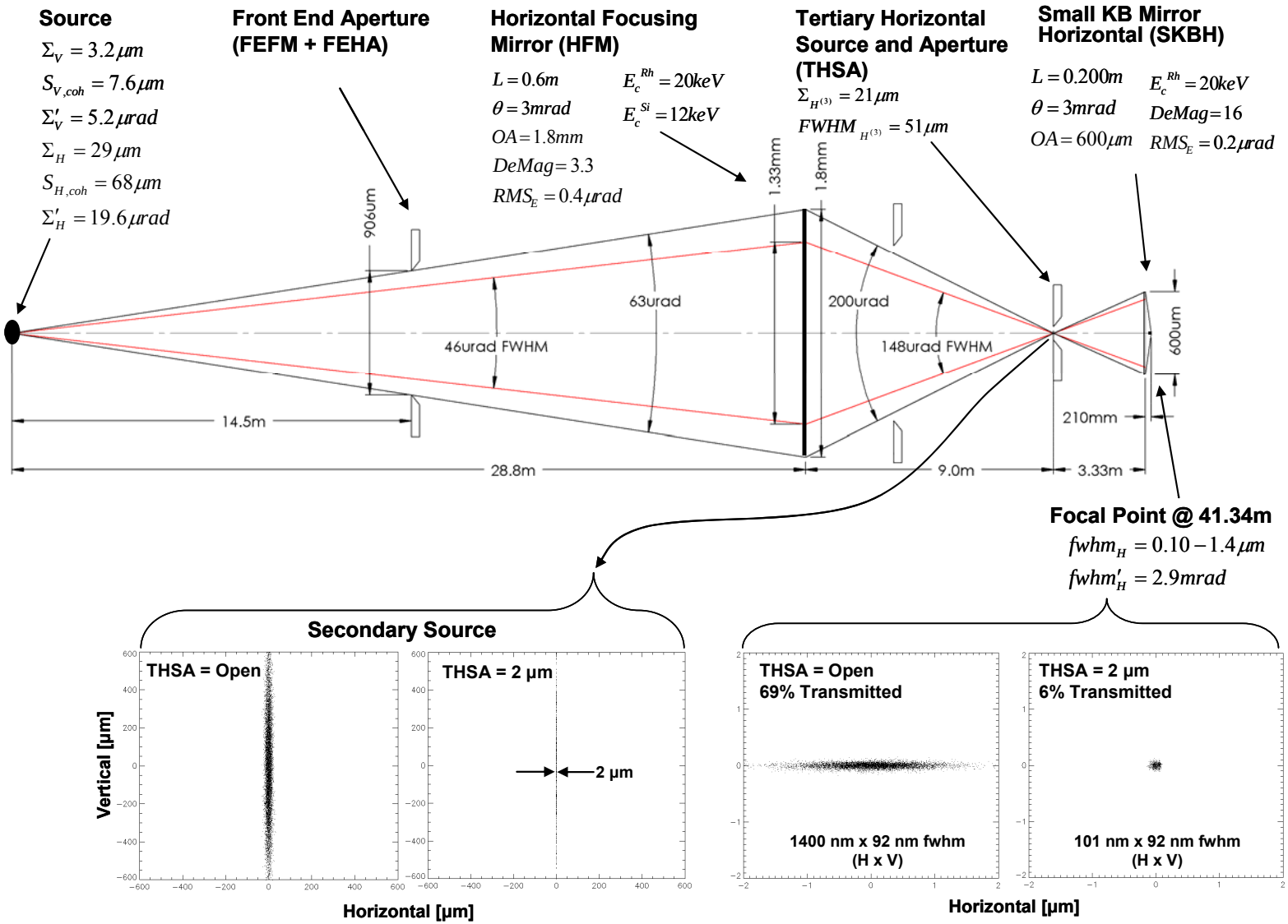

Figure 2.A.5. Optics layout and ray trace for a compound horizontal focusing at 76 m, focusing the beam to 1 nm with a working distance of 10 mm.

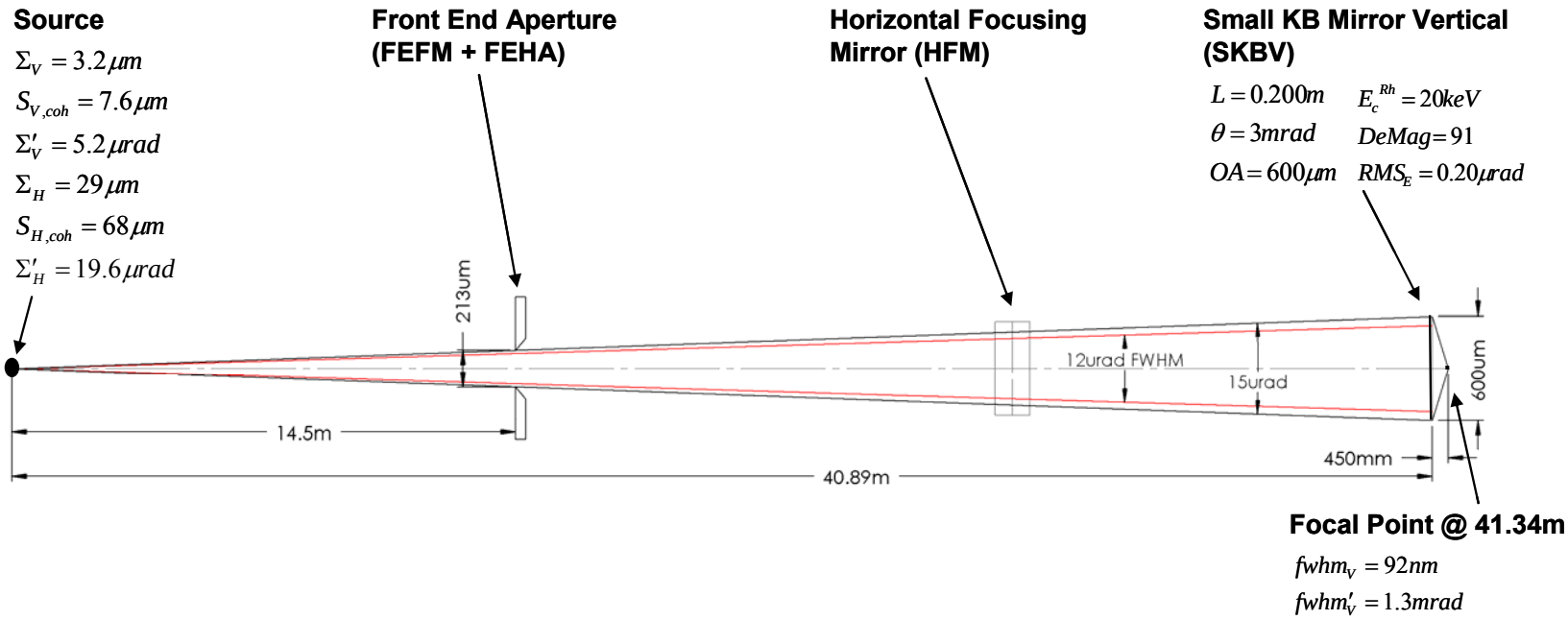

Figure 2.A.6. Vertical optics layout and ray trace for compound horizontal KB focusing mode for full-field imaging at 41m using a small vertical KB mirror, together with horizontal compound reflective optics.